12-16-2021

Numerical Simulation of a Cryogenic Spray

Neel Kishorkumar Shah
Embry-Riddle Aeronautical University, shahn3@my.erau.edu

NUMERICAL STUDY OF A CRYOGENIC SPRAY

By

Neel Kishorkumar Shah

A Thesis Submitted to the Faculty of Embry-Riddle Aeronautical University

In Partial Fulfillment of the Requirements for the Degree of

Master of Science in Aerospace Engineering

December 2021

Embry-Riddle Aeronautical University

Daytona Beach, Florida

NUMERICAL STUDY OF A CRYOGENIC SPRAY

By

Neel Kishorkumar Shah

This Thesis was prepared under the direction of the candidate's Thesis Committee Chair, Dr. Bertrand Rollin, Department of Aerospace Engineering, and has been approved by the members of Thesis Committee. It was submitted to the Office of the Senior Vice President for Academic Affairs and Provost, and was accepted in the partial fulfillment of the requirements for the Degree of Master of Science in Aerospace Engineering.

THESIS COMMITTEE

Rollin, Bertrand Digitally signed by Rollin, Bertrand Date: 2021.12.08 13:06:54 -08'00'

Chairman, Dr. Bertrand Rollin

Reda R.mankbadi Digitally signed by Reda R.mankbadi Date: 2021.12.08 17:23:05 -05'00'

Member, Dr. Reda Mankbadi

Birce Dikici Digitally signed by Birce Dikici Date: 2021.12.09 12:44:29 -05'00'

Member, Dr. Birce Dikici

Daewon Kim Digitally signed by Daewon Kim Date: 2021.12.09 13:10:09 -05'00'

Graduate Program Coordinator,
Dr. Daewon Kim

12/9/2021

Date

James W. Gregory Digitally signed by James W. Gregory Date: 2021.12.09 21:35:39 -05'00'

Dean of the College of Engineering,
Dr. James Gregory

12/09/2021

Date

Associate Provost of Academic Support,
Dr. Christopher Grant

Date

ACKNOWLEDGEMENTS

I want to express my sincere gratitude to my research advisor, Dr. Bertrand Rollin, for the continuous mentorship, guidance, and motivational support in completing my master thesis research. His knowledge and expertise helped me be diligent in delivering quality and excellence in this research.

Secondly, I also wanted to express my special thanks to the research committee members, Dr. Reda Mankbadi and Dr. Birce Dikici, who helped me achieve qualitative research standards. It would have become more challenging to move even a single step ahead without all the professors.

Finally, I would like to exhibit my deep and sincere regards to my parents Mr. Kishorkumar Shah and Mrs. Mrudulaben Shah, for their love, care, sacrifice, and constant reinforcement towards my higher education. Also, my sister Dr. Drashti Shah, for providing a spirited and inspiring outlook preserving my perseverance. Indeed, it wouldn't have been possible without all this hand behind.

ABSTRACT

Cryogenic sprays have many applications in modern engineering. Cooling of electronic equipment subject to high heat flows, surgical ablation of gastrointestinal mucosae or orbital maneuvering are a few examples of their versatility. However, the atomization of a cryogenic liquid is a complex process. During such an event, aerodynamic effects associated with secondary atomization are further affected by thermodynamic flashing. A better understanding of the characteristics of cryogenic sprays is then necessary to allow for improved design and optimization in applications. The overarching objective of this study is to document such characteristics. The numerical simulation was performed over cryogenic nitrogen spray using an Eulerian-Lagrangian approach. In other words, while the gas phase of the flow is treated as a continuum, the nitrogen droplets are tracked individually in a Lagrangian sense. Models for evaporation, atomization, and breakups capture the physical processes experienced by droplets along their pathways. In addition, turbulence in the flow is captured by the k-omega SST model. Simulations performed over a wide range of nozzle inlet pressure suggest that the spray cone angle tends to remain constant. In contrast, the diameter of droplets along the centerline of the spray reduces significantly. Finally, it was noticed that a higher concentration of liquid nitrogen is observed on a target plate as the nozzle inlet pressure increases.

TABLE OF CONTENT

LIST OF FIGURES

LIST OF TABLES

SYMBOLS

d_v	Droplet diameter of same volume
d_s	Droplet diameter of same surface
E	Energy
g	Gravitational Acceleration
P_∞	Atmospheric Pressure
p	Pressure
ρ	Density
S	Source term
$\bar{F}$	External Force
F_D	Drag Force
t	Time
$\bar{v}$	Velocity vector
σ	Surface Tension
μ_L	Dynamic Viscosity of the liquid
$\dot{m}_L$	Liquid mass flow rate
ΔP_L	Pressure Difference
ρ_L	Fluid density
θ	Time Scale
α	Mass Fraction
N_2	Liquid Nitrogen

x	Vapor quality
$\bar{\bar{\tau}}$	Stress tensor
G	Generation of Turbulent Kinetic Energy
Γ	Effective Diffusivity
Y	Dissipation rate
C_d	Drag Coefficient
Re	Reynolds Number
N	Molar Flux
C_i	Vapor Concentration
M	Molecular Weight
c_p	Heat Capacity
T	Temperature
h_{fg}	Convective Heat Transfer coefficient
u	Axial velocity
h_o	Thickness of the liquid film
d_o	Injector exit velocity
MPa	Million Pascals

ABBREVIATIONS

AIAD	Algebraic Interfacial Area Density
AMD	Arithmetic Mean Diameter
CHF	Critical Heat Flux
CFD	Computational Fluid Dynamics
D_{32}	Sauter Mean Diameter
DPM	Discrete Particle Method
FVM	Finite Volume Model
HRM	Homogeneous Relaxation Model
K	Kelvin
KHRT	Kelvin-Helmholtz Rayleigh Taylor
LED	Light Emmiting Diode
LISA	Linearized Instability Sheet Atomization
LN_2	Liquid Nitrogen
MPa	Million Pascal
psi	Pound per square inch (Pressure unt)
RANS	Reynolds Averaged Navier Stokes
SMD	Sauter Mean Diameter

SSD	Stochastic Secondary Droplet
SST	Shear Stress Transport
TAB	Taylor Breakup Model
TKE	Turbulent Kinetic Energy

1. Introduction

A dynamic collection of tiny fluid droplets disperses in a medium is known as a spray. The process of formation of such droplet particles is known as atomization. The atomization process is a disintegration of a liquid sheet by exposing it to high-velocity air or gas or through any external mechanical process generated by a rotating or vibrating device. The application of transforming the bulk liquid into this physical dispersion of particles in a fluid is crucial in several industrial sectors, agriculture, medicine, and many more field. Numerous spray devices like nozzles and atomizers have been developed based on application. The design of these nozzles is so that the spray characteristics change according to the application. Spray characteristics include drop size, spray pattern, spray angle, droplet velocity, and how the spray impacts the target surface.

Initially, the spray starts with a dribbling stage, but it transforms into a fully developed spray as the upstream pressure or the liquid injection pressure increases. The formation of a jet or the spray characteristics is also affected by external environment parameters like temperature, specific gravity, the viscosity of the fluid, and surface tension between the liquid and surrounding air (Hanson, 2020).

The pressure upstream of the nozzle also plays an essential role in the development of the spray. The spray tends to disintegrate more aggressively and delay forming a fully developed mist as the pressure difference increases at a constant atmospheric condition. The pressure difference is the difference in injection pressure and atmospheric pressure. As a result, the liquid jet disintegrates into a liquid film sheet in the fully developed spray, resulting in primary atomization and secondary atomization.

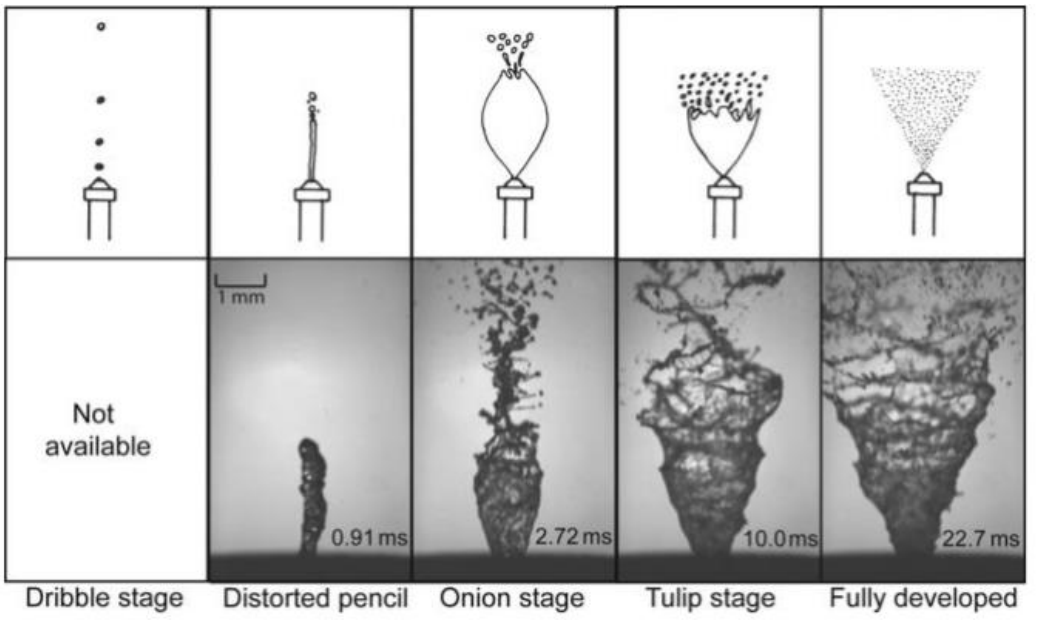

Figure 1.1 Stage of water spray formation (Fung et al., 2013)

The spray ability is also affected by the properties of the working liquid used in the spray. The fluid's specific gravity affects the overall mass flow rate of the fluid at the nozzle exit and finally affects the droplet diameter. So, for a given pressure, higher specific gravity reduces mass flow rate and hence lower mean droplet size. The high-density liquid jest does not atomize efficiently, but by changing the temperature, the viscosity of the flow, it can assist in promoting atomization. Temperature affects the spray pattern indirectly because the density and fluid surface tension decrease with an increase in temperature. Figure 1.2 shows the effect of temperature on the density of the water. The lower temperature will increase the fluid's viscosity, making the droplet stay together and form a larger droplet.

In industry, most spray application has unique requirements and specifications. This requirement includes nozzle type, spray pattern, size, cone angle, design, and spray attributes. So, it is crucial to select a specific nozzle while considering the environmental condition as well.

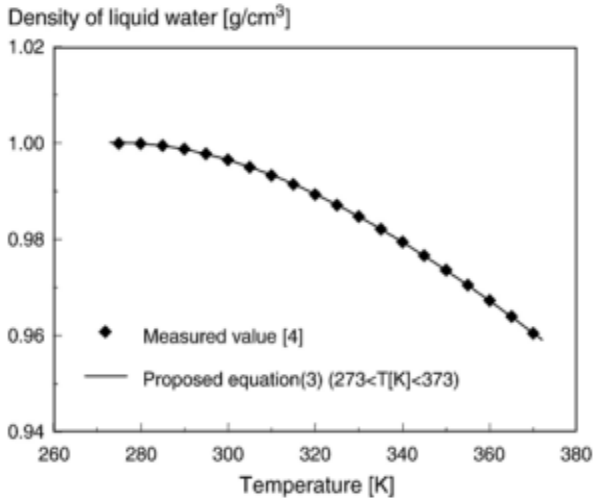

Figure 1.2 Change of density with temperature (Ishida et al., 2007)

Spray patterns are also formed based on the nozzle shape, as shown in Figure 1.3. The pattern creates a different impact on the target plate and different spray droplets diameter and other parameters. The flat fan spray is mainly used for continuous spray and efficiently covers every corner along the axial direction. It forms a standard distribution curve for the spray volume over the target plate, effective for road marking, food spraying, and many more application. The hollow cone nozzle covers the circular area over the target plate hence more effective at the circumference than the center of the cone.

In contrast, a full nozzle cone covers less space than the hollow cone nozzle, as it sprays evenly on the target object. Similarly, the atomizing hydraulic spray is primarily used for compressed air and cooling substance with evaporating fluid at much higher pressure (around 10 to 100 pound per square inch). The kinetic energy increases with increased stress, which allows the liquid to atomize into much smaller particles than a full cone nozzle. The pressure upstream of the nozzle may vary depending upon the application. The droplet size and spray pattern are crucial factors for this nozzle; they can be used in spray cooling. These parameters may help to reduce the NO_x or CO_x emission and the cooling tower gas. So, controlling droplets and optimal injector placement are essential keys for practical use.

.

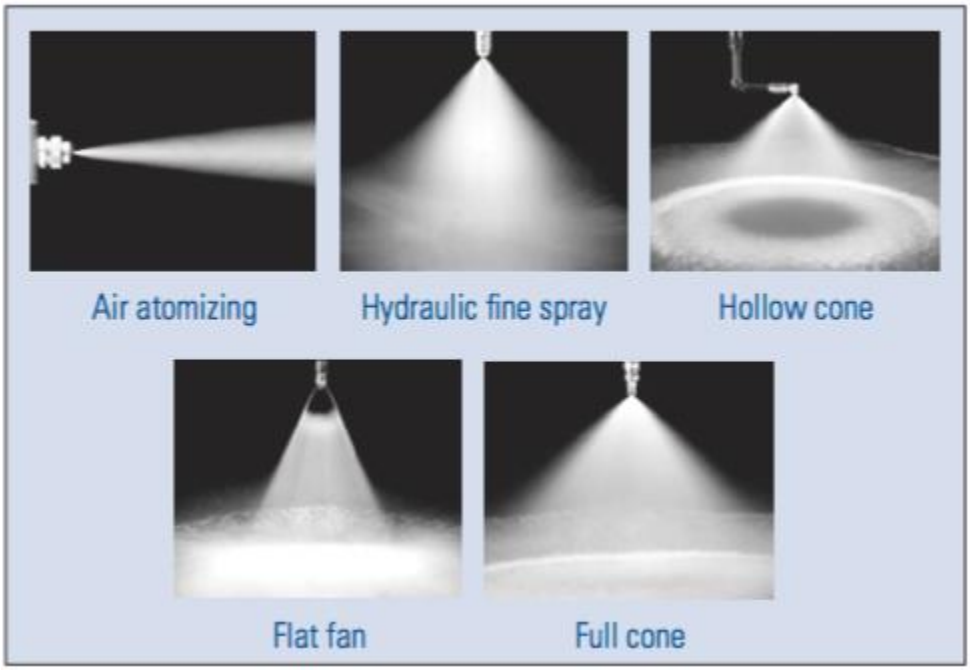

Figure 1.3 Spray patterns (Spraying Sytems Co, 2021)

Cryogenic nozzles must sustain extreme temperatures difference and mechanical conditions. Thermodynamics flashing plays a vital role in breaking particles and the aerodynamic breakup in the cryogenic spray. Thermodynamic flashing is for the liquid which has an exponential evaporation rate due to a pressure drop. The vapor phase production process is generally carried out by the thermodynamic and the mechanical non-equilibrium, created due to the significant difference between temperature and velocity of both phases. The increase of vapor bubbles is mainly due to the thermodynamic non-equilibrium. This non-equilibrium plays a crucial role in superheating the liquid above the saturation temperature.

There are a few other types of spray with different characteristics and can work more effectively and efficiently based on the implementation. Information (external conditions) or data (patterns) helps to alter the spray morphology. The important parameters like flow rate, upstream pressure, spray distance from the target helps us to design better nozzles more effectively, while atmospheric parameter like temperature, pressure, fluid density, surface tension play a crucial role in understanding the efficiency of the spray

There is continuous effort to monitor how to spray characteristics affect the combustion and evaporation effects over spray fields. The rate of combustion/evaporation is directly dependent on the surrounding temperature, droplet-size-distribution, droplet diameter, and many other fluid parameters (Holyst, et al., 2013). The rate of combustion/evaporation is faster if the spray field is covered with a smaller droplet diameter. A sufficient evaporation rate can be achieved by altering parameters like nozzle exit pressure, mass flow rate, and nozzle diameter to achieve an efficient and effective spray droplet-size distribution for a specified application. For example, the engine

injectors are designed to reduce the droplet volume or droplet diameter for maximum combustion rate, resulting in less carbon deposition.

Spray-cooling technology uses the fundamentals of evaporation principles. The rate of the phase change (evaporation) is a critical factor in understanding the reaction rate while the working fluid is liquid hydrogen or oxygen. The interest in spray cooling or cryogenic spray has been increasing due to a better understanding of the evaporation rate along with droplet size.

Cryogenic sprays are advanced spray technology that uses cryogenic fluid with a saturation temperature below 120 Kelvin as their working fluid for various applications. Cryogenic spray applications have been so far limited to aerospace engineering, electric cooling, or medical science. In aerospace engineering, the cryogenic wind tunnel is one of the applications of spray cooling. In the cryogenic wind tunnel, liquid nitrogen is sprayed into the control volume to increase the Reynolds number as much as the factor of seven with no significant change in the dynamic pressure and reduction in the driving power (Dress & Kilgore, 1984). Various cryogenic fluids like liquid hydrogen, nitrogen, oxygen, and methane are used in multiple applications based on their chemical composition.

The methane and hydrogen being highly flammable liquids, their usage remains limited. Liquid oxygen acts as an oxidizer which limits its use as a fuel. The application of liquid nitrogen is more widespread due to its inert properties among cryogenic fluids. The atomization process of cryogenic spray becomes challenging due to the combined effect of the mechanical breakup and thermodynamics flashing.

The increase in ambient pressure exerts a significant force on the bubble growth. As a result, the bubble radius varies during the flashing process for different ambient pressure (P_∞). The bubble expansion is controlled by heat transfer when the surface temperature reduces to its saturation temperature of the corresponding ambient pressure. This process is also known as the heat transfer-controlled domain. In the heat transfer domain, the pressure difference between the inside and outside of the bubble approaches zero, and gradually, the bubble growth rate reduces with respect to time. This process also delays the droplet breakup time.

Another critical parameter that also plays a crucial role in the field of cryogenic spray is Sauter Mean Diameter (SMD). This parameter helps to understand the average particle diameter of the dispersed fluid. SMD is calculated using the average surface area and the volume of the particle.

$$D_{32} = \frac{d_v^3}{d_s^2} \tag{1.1}$$

where d_v and d_s are calculated using average volume and surface area, respectively, this parameter further helps understand the evaporation rate and the mass transfer of the fluid into a vapor. Thus, SMD becomes a crucial factor when dealing with cryosurgery, in which the larger diameter of the particle can create substantial side effects which might be challenging to overcome. Furthermore, in cryosurgery, droplet distribution of the fluid is also crucial as it might affect other vital tissues in the body. In addition, the droplet distribution or the spray cone angle is greatly affected by the injection pressure and the nozzle type.

Currently, the application of spray cooling through cryogenic fluid has increased in electronic cooling applications. Due to high-performing computing operations, future

power electronic applications might require innovative technologies to remove high heat flux. Furthermore, it is essential to operate this application at low temperatures to increase the components' reliability, which results in increased efficiency (Jungho, 2006). As spray cooling provides the best combination of high Critical heat flux (CHF) removal efficiency, isothermality, and fluid inventory, it is preferred over any jet impingement cooling system. However, such spray's understanding is limited to some basic parameters, while a deep understanding would be required to calculate heat transfer, film thickness spray parameters, and patterns. Due to which it lacks in understanding the preliminary fundamental principle of such cooling spray and some failed commercial products, restrict its use in commercial applications.

CHF is the thermal limit of a scenario where phase change is caused due to heating, which has a steep decrease in heat transfer efficiency. The sudden mixing of the fluid occurs due to more efficient heat transfer and droplet turbulence (Zuber, 1959). Therefore, boiling heat transfer has played a promising role in the industrial heat transfer process in macroscopic heat transfers (heat transfer exchangers or fossil power plants) and microscopic heat transfer devices (pipes and microchannels for cooling electronic chips).

Due to such a growing number of applications across a wide range of industries, it becomes essential to characterize the formation of cryogenic spray better and qualify the properties. These are the over-arching motivations for this work.

2. Literature Review

As the interest in cooling technology development has recently increased, cryogenic spray has become essential for significant temperature reduction and high power density handling. Its practical high heat flux removal ability, evaporation rate, and large Reynolds number with low power consumption have created widespread attention.

2.1. Experimental Studies of Cryogenic Spray

Practical experiments are essential to understand the complex physics behind the cryogenic spray because it allows more accurate and descriptive results, which can further help to change the theories into a real-life application with few drawbacks.

2.1.1. Critical Heat Flux Effect

Spray cooling may reduce the over 33^{o} C of junction temperature and 35% power consumption compared to cooling with air (Cader et al., 2004). Spray cooling also allows precise temperature control with low inventory liquid because of its adequate high heat flux removal capacity in both single and two phases. Besides, spray cooling also provides a uniform cooling temperature over the targeted surface with low fluid inventory (Gao & Li, 2018). The initial step to understanding the spray cooling technology is to discover how the heated surface is affected. For this, numerous fundamental studies have been overseeing theoretically and experimentally, mainly focusing on crucial parameters affecting the impact dynamics and relevant heat transfer mechanism. There are four main aspects for the noticeable effect of cooling performance: spray characterization, nozzle parameter (it includes positioning and design), phase change, and enhanced surface. In compliance efforts, scientists have put a great effort into understanding the spray characterization, critical heat flux (CHF), and relevant cooling performance of spray

cooling (Toda, 1972). Further research found that the mean droplet velocity is the most promising parameter affecting the CHF, followed by mean droplet flux (Chen et al., 2002) while experimenting with all the parameters individually.

Ested, K. A. and Mudawar, I. (1995) experiments on spray cooling suggest that change in volumetric flux affects the boiling curve as it affects evaporation efficiency. This local volumetric flux change (change in Weber number) has a direct correlation with CHF. Sauter Mean Diameter (SMD) is dependent mainly on orifice diameter, Weber number, and Reynolds number.

2.1.2. Evaporation effect

Xue, R et al. (2019) have explained the effects of injection mass flow rate on evaporation rate, temperature distribution, and droplet distribution of the spray field using Computational Fluid Dynamics (CFD). In this study, the evaporation of the spray field and temperature distribution were clearly explained through experimental and numerical analysis. The intense evaporation produced by the fluctuation injection was mainly due to an increase in the velocity of the fluid in the spray. This velocity gives rise to Turbulent Kinetic Energy in the fluid particle, which may cause collision of particles, disintegrating or merge to form a new particle with different size, shape, and volume. Therefore, the average diameter is taken into consideration for all the developed particles. This average diameter is also known as Sauter mean diameter (Mugele & Evans, 1951), which was also calculated to understand the physics behind the droplet evaporation in the liquid nitrogen spray field. In other words, the Sauter Mean Diameter (SMD) is the diameter having the same volume to surface area ratio for the accounted particle.

$$SMD = \frac{d_v^3}{d_s^2} \tag{2.1}$$

where the d_v and d_s are the diameters of volume and surface diameter of the particle, these parameters were calculated by another method without any information about the physical properties of the droplet.

Evaporation cooling by liquid nitrogen spray is extensively used to achieve immediate cooling, thermal uniformity, and temperature accuracy in an ample space like a cryogenic wind tunnel (Fey, et al., 2003).

Xue, R et al. (2018) experimented with liquid nitrogen in atmospheric conditions to measure the effect of pressure difference over spray cone angle and Sauter Mean Diameter (SMD) D_{32} for different types of nozzle configuration. In addition, Droplet spatial distribution was evaluated at various locations in the axial direction to understand SMD distribution over the spray field.

According to Lefebvre and McDonell (2017), the SMD was calculated using the following equation for the pressure swirl nozzle:

$$SMD = 2.25\ \sigma^{0.25}\ \mu_L^{0.25}\ \dot{m_L}^{0.25}\ \Delta\ P_L^{-0.25} \rho_L^{-0.25} \tag{2.2}$$

2.1.3. Reynold Number Effect

Initially, the common problem faced by wind tunnels was low Reynolds number, flow steadiness, and a few other interferences. To overcome these problems, NASA proposed a cryogenic wind tunnel for high Reynolds number testing. A cryogenic wind tunnel offers the unique ability to achieve full-scale Reynolds number with appropriate test sections, dynamic pressure, and driving power. The use of such a wind tunnel has a different effect on Reynolds number, flow velocity, and aeroelasticity (Lawing & Kilgore, 1986). Boundary layer development was identical for ambient and cryogenic conditions; however, it has significantly reduced the drive-power and fan-speed. As

cooling with LN_2 is more practical, it became easy for instant cooling of environment and automatic temperature control.

2.1.4. Flashing (Flash Boiling) Effect

Flashing spray occurs when a high-pressure liquid is injected into a low-pressure environment to make the liquid superheated, characterized by explosive atomization of superheated liquid to generate fine droplets and accompanied by evaporation of these droplets leading to exceptional low fluid droplet temperature (Zhou et al., 2012). Thermodynamic instability to break the liquid jet is considered for flash boiling atomization. As the heated liquid is accelerated through the injection nozzle, its pressure decreases. If this pressure falls sufficiently below its saturation vapor pressure, it can result in rapid boiling (Reitz, 2007), known as nucleate boiling.

Atomization of some droplets mainly occurs due to nucleate boiling also. Flash boiling occurs in three stages; initially, the liquid jets form bubble nucleation, resulting in the bubble's growth inside the droplet, and finally, a two-phase flow. Bubble nucleating is the process of rate-controlling for the lateral spread of the spray and fully flash boiling. Once the bubble nucleation sites start developing, the fluid pressure fluctuations can result from either collapse or expansion. Moreover, flash boiling leads to more satisfactory and wider atomization in the control volume with slow droplet speed. Therefore, the understanding of bubble formation even becomes more crucial for flash boiling.

Rees, A. et al. (2020) generated a highly superheated flashing LN_2 spray, known as fully flashing squirt, according to Cleary et al. (2007). The experiment shows a sudden decrease of velocity along with the radial distance near the nozzle exit because of the

horizontal momentum direction for the widening of the spray in that region. At superheated levels, nucleation and bubble growth can drastically reduce the speed of sound for two-phase flow. The internal energy of LN_2 was transformed into kinetic energy near the nozzle exit, resulting in more vertical velocity downstream of the nozzle orifice (Figure 2.1), resulting in expansion of the spray region.

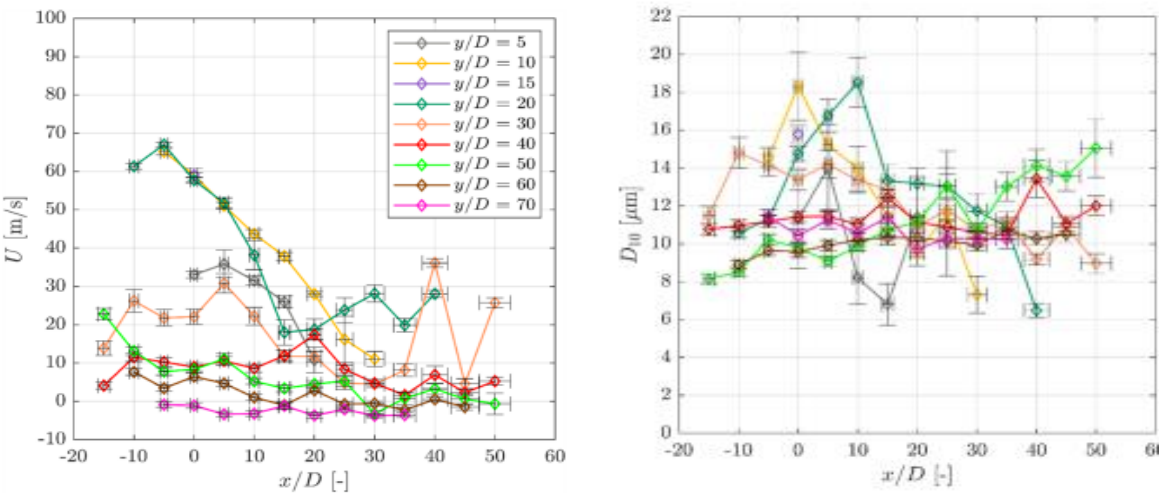

Figure 2.1 Spatial Distribution of mean vertical velocity (left) and Arithmatic Mean Diameter (right) in fully flashing LN_2 spray (Rees, et al., 2020)

As the horizontal speed along the injector axis is significantly reduced, it leads to a reverse flow far downstream. This decelerated flow interacts with secondary droplets formed by upstream flowing liquid. This interaction leads to further breaking up into tiny satellite droplets. A significant decline of the droplet Arithmetic Mean Diameters (AMDs) (Figure 2.1) of LN_2 spray was observed due to the considerably higher degree of superheat. This rise in temperature gave rise to stronger atomization by evaporation of the droplets which is also known as flash boiling.

2.1.5. Spray Cooling Efficiency

Researchers perform experimental studies better to understand the spray cooling efficiency over the spray region. Hou, Y. et al. (2014) experimented with the refrigerant coolant (R134-a) fluid to study spray cooling efficiency and the target surface temperature with heat transfer coefficient. This experimental study indicates that the convection heat transfer limits the impact of flow rate on heat transfer in the initial stage. Yet, the phase change generated due to evaporation, nucleates boiling, and the secondary nucleation of liquid thin film on the target surface enhances the heat transfer condition, increasing heat flux. Figure 2.2 shows the effect of phase change on heat transfer as it has a steep decline in heat transfer coefficient. Toh et al. (2010) used the same fluid in the experiment to understand the effects of mass flow rate, nozzle inlet pressure, and chamber pressure over spray cooling for high power devices.

It was observed that the more significant flow rate encourages an even distribution of the temperatures on the target surface. This temperature distribution may improve heat transfer conditions but at the cost of system efficiency (Hou, et al., 2014). Also, a high mass flow rate increases the formation of larger droplets, reducing the vaporization efficiency of forming a thick liquid film over the target plate. High nozzle inlet pressure can compensate for this downside of high mass flow rate, which increases droplet velocity and promotes fine droplets. This increase in droplet velocity intensifies the heat transfer rate and droplet distribution, resulting in better distribution overheated surface. This also shows that the volumetric flow rate has a significant influence on spray cooling performance. Further analysis suggested that chamber pressure doesn't significantly affect the temperature of the target plate.

However, according to the experimental research by Chow L. C. et al. (1995), the maximum effectiveness of the LN_2 spray cooling did not increase above 35%. Therefore, the lack of liquid was not the leading cause of CHF. Instead, the CHF is caused by the inability of the fluid to reach the surface at a sufficient rate.

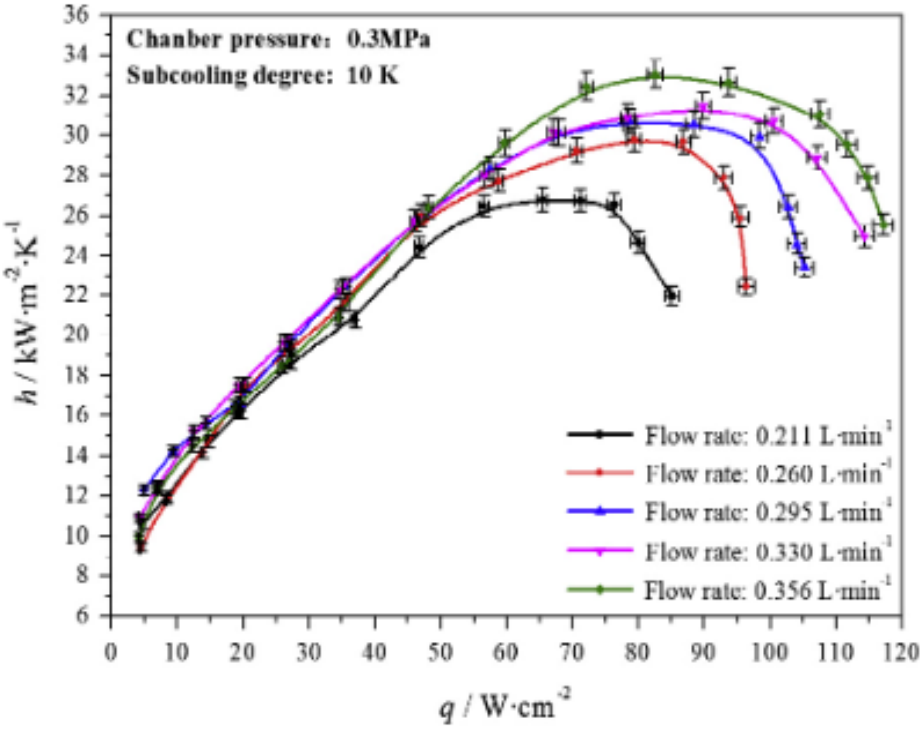

Figure 2.2 Heat transfer coefficient for discharge coefficient (Hou, et al., 2014).

The above literature found a promising conclusion over understanding the parameters that affect the spray morphology for LN_2 spray. However, in a practical turbulence spray field of liquid nitrogen, the droplet activity, rate of evaporation, and the mixing of liquid and vapor phases coincide and couple tightly. The dominant input parameter affecting fluid nitrogen spray characteristics is the upstream pressure, leading to more substantial cavitation (Zeng & Lee, 2001), which costs more heavily.

Liquid Nitrogen's high cost and maintenance make it more challenging to perform the practical test by varying various input parameters. The best way to overcome such a problem is to solve the spray field computationally. It will prevent hazardous situations and reduce the cost of setting up the apparatus, and it will help to understand every parameter separately.

2.2. Numerical Study of Cryogenic Spray

Numerical simulation helps to understand the physical phenomena and their interaction more accurately. Compared to experiments, CFD simulations were able to gain some new insights into physics considering the complex aerodynamics and thermodynamics interaction in the spray field. Several theories and equations are proposed to validate the spray cooling phenomenon and instabilities in the spray field.

2.2.1. Computational Models for Aerodynamic and Thermodynamic Interaction

For aerodynamic interaction, the Kelvin-Helmholtz (K-H) instability model is generally used to explain the aerodynamic interaction at the liquid-gas interface and predict the breakup of a high-pressure liquid jet (Zeng & Lee, 2001). A commonly used breakup model is the Taylor Analogy Breakup (TAB) model, which explains the drop behavior by comparing it with the oscillating spring-mass system. Zeng and Lee (2001) used a modified TAB model with a single bubble assumption to predict the fuel atomization. The Rayleigh Taylor model was recently adopted, a modified K-H wave model incorporated with the TAB model.

For thermodynamics interaction, researchers were mainly focused on the fuel flashing. Kim and Park (2018) developed a flash breakup model and used it to form a thermodynamic-mechanical breakup model. This breakup module was used to predict

flash boiling spray. This whole model was developed using Rayleigh-Plesset equations in the gasoline flash breakup model to predict the bubble growth inside the droplet. When the void fraction exceeds the critical value, a breakup is expected. Gartner, J. W. et al. (2020) presented an Eulerian/Lagrangian particle tracking approach with a subcooled and superheated evaporation model to model flash boiling spray. The Homogeneous Relaxation Model (HRM) was introduced, which considers that the mass, momentum, and energy transfer happens rapidly between the equilibrium phases (Chen, B. et al., 2017). On the other side, Zapolski, D. P. et al. (1996) proposed the Homogeneous Relaxation Model, which considers non-equilibrium vapor generation, and the instant vapor mass fraction would achieve an equilibrium state in a suggested timescale.

2.2.2. Turbulence Modeling for Sprays

The concept of a turbulent flow is not yet fully understood, neither mathematically nor by an intuitive method. Therefore, it is still challenging to achieve high accuracy in predicting any engineering flow. Researchers have created various turbulent models based on the boundary condition and flow type to predict the acceptable results for the turbulent flow region numerically. Eulerian-lagrangian, k-epsilon, and k-omega are a few turbulent models that give the most accurate results for spray simulation when compared to the experimental results. The Shear Stress Transport (SST) equation was incorporated with k-omega turbulent models to obtain more stable results for turbulent flow (Menter, 1994).

Gimeno, J. et al. (2014) compared all the Eulerian spray atomization models to justify the best model for diesel spray. It was found that the k-omega SST model gave accurate results not only for the internal flow but also for spray development. Further to

understand the microscopic detail of the spray, the Discrete Particle Method (DPM) was also introduced, which provides the information for every individual particle present in the control volume. According to Kumar, N. and Puranik, B. (2017), an Euler-Lagrangian method incorporated with DPM proves to be a more accurate model than a single-phase model for a low particle volume concentration of around 0.5%. Moreover, it can simulate the particle trajectory in an uninterrupted flow (Ishak, et al., 2018). Previous studies also show that DPM has delivered accurate and more reliable results to conceptualize practical scenarios.

2.2.3. Computational Models for Cryogenic Spray

Chen, J. et al. (2020)used an Algebraic Interfacial Area Density (AIAD) model integrated with the Homogeneous Relaxation Model (HRM) framework to simulate a 2-D cryogenic spray. The K-H instability principles were represented using the AIAD model. The significant results found that the length of the intact core was comparable to previous studies, which shows that the model was able to show both the effects of aerodynamic instability and thermodynamics interaction (Chen, J. , et al., 2020). Gartner, J. W. et al. (2020) also computed a 2D model of cryogenic spray to know the effect of mass flow rate, which was further compared to his experimental study showing the effect of flash boiling of Liquid nitrogen spray (Figure 2.3). The simulation increased the evaporation mass flow rate as the spreading of the spray region was below the prediction to achieve the increase in evaporation mass.

HRM estimates the rate at which the local vapor quality approaches the equilibrium vapor quality. The rate of change of vapor quality can be mathematically represented by:

$$\frac{Dx}{Dt} = \frac{\bar{x}-x}{\theta} \tag{2.3}$$

Θ is the time scale calculated as:

$$\Theta = \Theta_0 \alpha^{-0.54} \Psi^{-1.76} \quad (2.4)$$

where, $\Theta_0 = 3.84 * 10^{-7}$; $\Psi = \frac{|P_{sat} - p|}{p_{crit} - p_{sat}}$; and $\alpha = \alpha_{N2} + \alpha_{O2} + \alpha_{v.}$

These significant values were effectively evaluated for pressure higher than 10 bar (Kumar & Puranik, 2017).

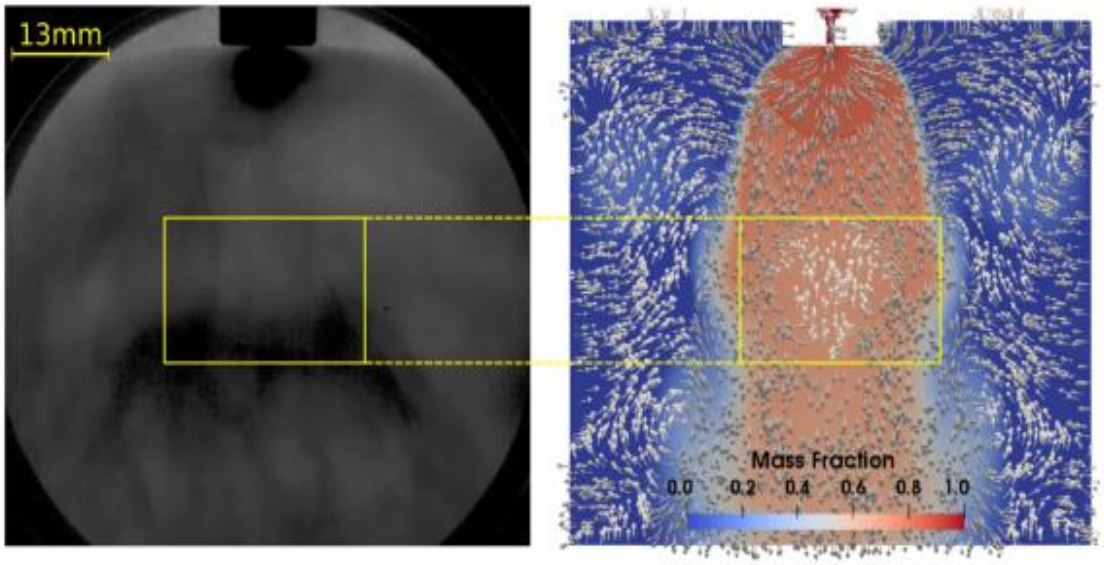

Figure 2.3 Shadow experimental result and Numerical analysis of mass fraction (Gartner, et al., 2020).

2.2.4. Numerical Analysis Over the Parameters Affecting the Spray

Xue, R. et al. (2018) performed numerical analyses using the Eulerian-Lagrangian approach to various model frequencies and amplitude fluctuations inlet mass. The experiment found that when the liquid nitrogen spray is in the fully developed stage, the

outlet temperature and the evaporation rates also fluctuate around the average value at the same inlet mass flow rate (Xue, et al., 2019). Due to the fluctuation in injection mass flow rate, the corresponding average Turbulent Kinetic Energy (TKE) of the spray area was increased, resulting in a comprehensive increase in evaporation of the spray field. This evaporation also reduces the droplet size due to stronger TKE resulting in a negligible effect of injected mass rate fluctuation directly on the droplet size.

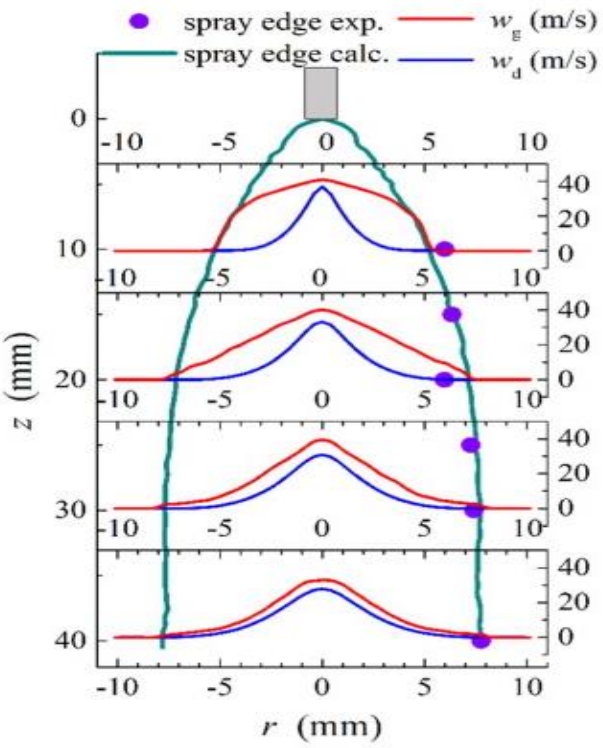

Figure 2.4 Velocity profile for liquid and gas (Chen, B. et al., 2017)

In the work of Liu, H. et al. (2017) of multiphase spray cooling with a numerical model, an Euler-Lagrangian approach was carried out to describe the spray cooling process. The k- epsilon turbulence model was applied for describing the turbulence characteristics of the spray flow. It also used a discrete phase model solved by the

Lagrangian method to solve the droplet diameter distribution. The result showed that the wall temperature increased along with the spray height creating a high heat flux. Moreover, as the heat flux increases, while the heat flux coefficient is linear, the effect of spray height reduces on the wall temperature. Tarantino, L. et al. (2010) investigated the Soave Redlich-Kwong Ideal gas model over the thermodynamically gas, liquid nitrogen jet. This numerical study was mainly to understand the effect on density over the spray field.

Chen, B. (2017) implemented a hybrid vortex method incorporating the Euler-Lagrangian method for cryogenic spray cooling with R134-a refrigerant cooling fluid. This numerical analysis showed the time-averaged velocity distribution for simulated gas and liquid (Figure 2.4). However, this precise velocity distribution near the nozzle exit was not explained successfully in the experimental results.

3. Computational Model

The turbulent spray evaporation is a mixture of various reactions or transformations coinciding in the spray field. This phenomenon results to further atomization of the working fluid. This atomization occurs mainly due to aerodynamic or flashing interaction, droplet evaporation, dispersion, and the interaction between liquid and gas-phase flow. So, many models are necessary to capture the physics at play adequately.

Turbulence models aim at predicting pressure, temperature, velocity field without calculating the pattern of the entire turbulent flow. Therefore, a turbulence model such as Reynolds-Averaged Navier stokes (RANS) needs a sub-model to solve further fluid flow. These sub-models include k-omega, k-epsilon, and many other models to understand convergence and turbulent flow better. According to the experimental outcome, the k-omega model was more accurate and had promising results (Gimeno et al., 2014). Furthermore, this model was also integrated with Shear Stress Transport (SST) model, which combines k-epsilon for the outer boundary layer and k-omega for the inner boundary layer (Menter, 1994). The evaporation model explains the evaporation effect occurring due to temperature differences. The evaporation factor becomes critical due to the high-temperature difference between the subcooled liquid nitrogen and atmospheric condition.

Finally, as the liquid cryogenic fluid is sprayed into the atmosphere, it will start vaporizing after a certain period due to the Leidenfrost effect. Therefore, a Discrete Particle Model (DPM) is used to consider all the transformations occurring from the injection of liquid fluid to its evaporation. It contains various spray models like atomization, dispersion, thermophoretic force, temperature-dependent latent heat. The

turbulence carries out the other mixing process. Additionally, both phases are affected through mass, momentum, and heat transfer. The heat transfer among the droplets increases the energy and the temperature forcing it to evaporate. The drag force creating the transfer of momentum changes the turbulent flow pattern. There are various models for considering each of the parameters.

Ansys Fluent was used to simulate the numerical study for the research. Also, it solves the turbulent flow equations (Ansys-Inc, 2009), which are described in the following section.

3.1. Governing Equations

The governing equations dictate how the flow evolves through space and time. First, the initial boundary condition is defined to solve any turbulent flow using Navier-Stokes equations. The equation consists of basic conservation principles of mass, momentum, and energy are computed using Finite Volume Model Scheme. Also, additional transport equations are also needed due to evaporating particles (Ansys-Inc, 2009).

The continuity, momentum, and energy equations are described as follows in Equations 3.1a to 3.1c.

$$\frac{\partial \rho}{\partial t} + \nabla \cdot (\rho \vec{v}) = S_m \tag{3.1a}$$

$$\frac{\partial}{\partial t}(\rho \vec{v}) + \nabla \cdot (\rho \vec{v} \vec{v}) = -\nabla p + \nabla(\bar{\bar{\tau}}) + \rho \vec{g} + \vec{F} \tag{3.1b}$$

$$\frac{\partial}{\partial t}(\rho E) + \nabla \cdot (\rho \vec{v} E) = \nabla.(q) + S_h \tag{3.1c}$$

For the given set of equations, the ρ, υ, g is the density, velocity of the fluid, and the gravitational acceleration acting on the particles respectively. These are also the primary variable defining the governing the transport equations and needed to complete the

system of equations. The S_m and S_h terms are the source terms set to linearize source terms while solving the equations for simplicity and faster convergence. Furthermore, the $\vec{F}$ is the total force applied by the gravitational body force and the external body force. $\bar{\bar{\tau}}$ is the stress tensor; given by:

$$\bar{\bar{\tau}} = \mu\left[(\nabla \vec{v} + \nabla \vec{v}^T) - \frac{2}{3}\nabla . \vec{v} I\right] \quad (3.2)$$

Ansys Fluent provides the platform to numerically solve such a set of Equations (3.1a-3.1c) using Reynolds Averaged Navier-Stokes equations (RANS). Furthermore, as Discrete Particle Tracking is enabled, the conservation of species equation is also implemented. For our problem of interest, the species transport equation is given below is also solved:

$$\frac{\partial}{\partial t}(\rho Y_i) + \nabla.(\rho \vec{v} Y_i) = -\nabla.\vec{J}_i + R_i + S_i \quad (3.3)$$

In this equation, *i* denotes the number of species, R_i is the net rate of species production, and Yi is the local mass fraction of each species through the convection-diffusion equation.

The $\bar{\bar{\tau}}$ represents the Reynolds stress tensor, J_i is the turbulence flux are unknown terms which can be further solved using the turbulence sub-model. These new terms are necessary to close the system of equations for each time step (Ansys-Inc, 2009).

3.2. Turbulence Modelling

The RANS equations are the averaged equations of motions used for fluid flow. The RANS equations primarily describe the turbulent flow, including some additional terms

in momentum equations called Reynolds stress terms. These unknown terms were used in the turbulent model to represent the effect of turbulence.

The RANS equations used by Fluent are as follows:

$$\frac{\partial \rho}{\partial t} + \frac{\partial}{\partial x_i}(\rho u_i) = 0 \tag{3.4}$$

and,

$$\frac{\partial}{\partial t}(\rho v_i) + \frac{\partial}{\partial x_j}\left(\rho\, v_i v_j\right) = -\frac{\partial p}{\partial x_i} + \frac{\partial}{\partial x_j}\left[\mu\left(\frac{\partial u_i}{\partial x_j} + \frac{\partial u_j}{\partial x_i} - \frac{2}{3}\delta_{ij}\frac{\partial u_i}{\partial x_i}\right)\right] + \frac{\partial}{\partial x_j}\left(-\rho\overline{u'_i u'_j}\right) \tag{3.5}$$

These RANS equations is coupled with two sub-models to close the equations system: k- epsilon and k- omega equations. The first model uses a two-equation model of Turbulent Kinetic Energy and dissipation rate equations with a faster convergence rate. The latter model is used in most turbulence models because of its high accuracy for no-slip wall conditions. It is further integrated with SST sharp interface, which includes Reynolds stress equations. This interface solves both the models, i.e., k-epsilon for outer Boundary Layer (B.L.) and k-omega for inner B.L. Ansys fluent can solve these equations computationally (Ansys-Inc, 2009).

3.2.1. The k-omega Model

The k-omega is a widely used turbulence model because of its relatively high accuracy among the turbulence sub-model. The k-omega turbulence model is typically a two-equation turbulence model, which incorporates an approximation of Reynolds Averaged Navier Stokes (RANS) equations. This model aims to predict the turbulent

flow using two partial differential equations, solving for two variables k- being the Turbulence Kinetic Energy and omega being the specific dissipation rate.

The standard k- omega model is a low Reynolds number model generally used for low Reynolds number flow. The flow has a relatively thick boundary layer, and the viscous sub-layer can be resolved. It provides the best near-wall treatment. The standard k- omega model is further modified with the Shear Stress Transport (SST) equation to increase the accuracy in the outer boundary layer region, which is explained in the following section.

Turbulence Model Equations used by Ansys Fluent are:

$$\frac{\partial}{\partial t}(\rho k) + \frac{\partial}{\partial x_i}(\rho k u_i) = \frac{\partial}{\partial x_j}\left(\Gamma_k \frac{\partial k}{\partial x_j}\right) + G_k - Y_k + S_k \tag{3.6}$$

$$\frac{\partial}{\partial t}(\rho \omega) + \frac{\partial}{\partial x_i}(\rho \omega u_i) = \frac{\partial}{\partial x_j}\left(\Gamma_\omega \frac{\partial \omega}{\partial x_j}\right) + G_\omega - Y_\omega + S_\omega \tag{3.7}$$

Equation 3.6 and 3.7 describes the turbulence kinetic energy and the specific dissipation rate equation, respectively. The terms G_k and G_ω represent the generation of turbulence kinetic energy due to mean velocity gradient and omega, respectively. Γ_k and Γ_ω are the corresponding effective diffusivity of k and omega. Y_k and Y_ω represent the dissipation of k and omega due to turbulence. S are the other source terms that may add towards the production or dissipation of k or omega (Wilcox, 2008).

The effective diffusivity terms in k-omega can be represented as:

$$\Gamma_k = \mu + \frac{\mu_t}{\sigma_k} \tag{3.8}$$

$$\Gamma_\omega = \mu + \frac{\mu_t}{\sigma_\omega} \tag{3.9}$$

In this equation, the σ is the turbulent Prandtl number for the corresponding suffix. μ_t is the turbulence viscosity computed by:

$$\mu_t = \alpha^* \frac{\rho k}{\omega} \tag{3.10}$$

The coefficient α^* damps the turbulence viscosity causing a low-Reynolds number correction. The production of turbulence kinetic energy ($G_{k\text{-}\omega}$) can be calculated as

$$G_k = -\overline{\rho u'_\iota u'_j} \frac{\partial u_j}{\partial x_i} \tag{3.11}$$

and,

$$G_\omega = \frac{\omega}{k} G_k \tag{3.12}$$

The turbulence dissipation equations are given by:

$$Y_k = \beta^* \rho k\, \omega \text{ and } Y_\omega = \rho \beta \omega^2 \tag{3.13}$$

The above equations are simutaneously solved to perform k-omega simulations. However, these equations don't perform well in the far-field region of the control volume. Hence, SST formulation combines the best of two models (k-omega and k-ε turbulence model).

3.2.2. The k-omega SST Modeling

The SST k-omega turbulence model is a two-equations eddy-viscosity model used for various aerodynamic applications. It is a hybrid model of Wilcox k-omega and the k-epsilon equations. The SST formulations change to k-epsilon in the free stream, which overcomes the k-omega limitation of being sensitive to the free-stream turbulence properties at the inlet. In addition, despite producing significant turbulence levels, it constantly delivers high accuracy to expense ratio. This model considers the motion of principle shear stress for poor pressure gradient boundary layers.

The equation used to further modify the k-omega equations by integrating the SST are listed below:

- Kinematic Eddy Viscosity

$$\upsilon_T = \frac{\alpha_1 k}{\max(\alpha_1 \omega, SF_2)} \tag{3.14}$$

- Turbulent Kinetic Energy

$$\frac{\partial k}{\partial t} + U_j \frac{\partial k}{\partial x_j} = P_k - \beta^* k\omega \frac{\partial}{\partial x_j}\left[\upsilon + \sigma_k \upsilon_T \frac{\partial k}{\partial x_j}\right] \tag{3.15}$$

- Specific Dissipation Rate

$$\frac{\partial \omega}{\partial t} + U_j \frac{\partial \omega}{\partial x_j} = \alpha S^2 - \beta \omega^2 + \frac{\partial}{\partial x_j}\left[(\upsilon + \sigma_\omega \upsilon_T)\frac{\partial \omega}{\partial x_j}\right] + 2(1 - F_1)\sigma_{\omega 2}\frac{1}{\omega}\frac{\partial k}{\partial x_i}\frac{\partial \omega}{\partial x_i} \tag{3.16}$$

In this set of equations coefficient $\alpha_1 = 0.55$, $\beta_1 = 0.075$, $\beta^* = 0.09$, $\sigma_{\omega 2} = 0.5$. Further details about the coefficient and its auxiliary relations can be found in (Menter, 1993).

3.3. Discrete Phase Model (DPM)

The liquids phase of the cryogenic fluid is sprayed into the domain, which is further converted to gas-phase within a fraction of seconds. In practical operation, the interaction of both the steps affects the evaporation process and atomization, which must be considered. The pressure at which the liquid is released in the atmosphere allows the fluid to evaporate and provides the necessary momentum to accelerate the gas phase. Thus, it becomes vital to consider all the phenomenon occurring during the turbulent spray evaporation. The significant occurrence taking place during the initial stage of injection are dispersion, atomization, evaporation.

Initially, the liquid cryogenic fluid is injected or sprayed into the domain. This fluid is stored at a high pressure to maintain its liquid state. Once the liquid is exposed to the

atmosphere, it is evaporated, instantly converting into a gaseous phase. The stress and the velocity differences create the instabilities resulting in atomization and primary breakup of the liquid sheet into the droplets at the liquid-gas interface. Moreover, the evaporation rate gradually increased during the initial stage

The momentum of these droplets is transferred to kinetic energy, accelerating the gaseous particles further downstream. This Turbulent Kinetic Energy (TKE) gave rise to intensive evaporation induced by fluctuating injection. Also, there are high possibilities of increasing droplet evaporation due to this Turbulent kinetic energy. Moreover, the sudden increase in temperature forces the liquid droplet to evaporate at the liquid-gas interface. This evaporation creates a thin gas layer around the droplet resulting in the Leidenfrost effect.

There are two main approaches to model a fluid flow: Euler-Euler or Euler-Lagrangian approach. In the Euler-Euler approach, Navier-Stokes equations are solved for both phases considering both the phases as a continuum. Alternatively, the Euler-Lagrangian approach handles the gas phase as a continuum while the liquid phase has many discrete particles and tracks each particle's pathway. As a small amount of liquid is dispersed in the control volume, the Euler-Lagrangian approach is used for discrete phase modeling. The governing equations used to describe atomization and evaporation are discussed in the following section.

3.3.1. Particle Motion Equations

The equation of motion describes the path of the discrete phase particle or the droplet in the Lagrangian frame as a function of time. The trajectory (acceleration) equation for a particle is given by:

$$\frac{du_p}{dt} = F_{D\,(u-u_p)} + \frac{g_x(\rho_p - \rho)}{\rho_p} + F_x \tag{3.17}$$

In this equation, the $F_{.D}\,(u\text{-}u_p)$. is the drag force applied per unit particle mass, and the F_x is the additional force per unit mass acting on the particle. Here, u and $_{up}$ are the phase and particle velocity respectively. The second term is the buoyancy term.

In the Equation 3.17, F_D can be calculated using:

$$F_D = \frac{18\mu}{\rho_p d_p^2}\frac{C_D Re}{24} \tag{3.18}$$

where μ is the kinematic viscosity, ρ and ρ_p is the fluid and particle density, respectively, (Ansys-Inc, 2009).

The Reynolds number is defined as:

$$Re = \frac{\rho d_p |u_p - u|}{\mu} \tag{3.19}$$

where d_p is particle diameter and u is the velocity. The drag coefficient C_d can be calculated using various drag coefficient laws. The most preferred ones are the spherical drag law and dynamic drag model. The former method is mainly applied for smooth particles, while the latter model accounts for various droplet shapes and sizes. During the initial breakup, the spherical droplet passes through the gas domain, which changes the condition for a high Weber number.

As the drag coefficient is highly dependent on the droplet's shape, the dynamic drag model accounts for the distortion effect. If the droplets are assumed to remain spherical throughout the domain, the drag of the droplet can be calculated by Equation 3.20 (Ansys-Inc, 2009):

$$C_{d,sphere} = \begin{cases} 0.424 & Re > 100 \\ \frac{24}{Re}\left(1 + \frac{1}{6}Re^{\frac{2}{3}}\right) & Re \leq 1000 \end{cases} \quad (3.20)$$

However, a large Weber number can distort the droplet shape. Therefore, it might be possible that the sphere can be converted into a disc shape droplet, resulting in high drag compared to a spherical droplet. As a result, the dynamic drag model is introduced, which considers this effect of evaluating drag coefficient using Equation 3.21 where y is droplet distortion.

$$C_d = C_{d,sphere}(1 + 2.632y) \quad (3.21)$$

3.3.2. Heat and Mass Transfer

The effect of the continuous phase can be by modeling the reacting particle or the droplet. Ansys fluent provides a variety of particle types depending on how heat and mass transfer occurs in the particle or gas phase. The "Droplet" is selected as a particle type during the numerical simulation due to the evaporation condition in the droplet.

- Inert heating and cooling

The heating or cooling process occurring without any mass transfer in the domain is known as Inert Heating and Cooling for Ansys fluent (Ansys-Inc, 2009). It is operational until the temperature of the droplet reaches the vaporization or the evaporation temperature.

- Droplet Evaporation

The prediction of evaporation is initiated when the droplet temperature is between the evaporation temperature and the boiling temperature with mass transformation. The mass

transfer rate can be determined by the gradient diffusion, with the flux of the droplet vapor into the gas phase.

$$N_i = k_c\left(C_{i,s} - C_{i,\infty}\right) \tag{3.22}$$

where N is the molar flux, k is the mass transfer coefficient, and C is the vapor concentration (for the droplet surface(s) and gas (∞)). This mass transfer coefficient can be calculated using the Sherwood number correlation. And the vapor concentration can be obtained by modifying the Ideal gas equation.

The change in mass fraction of the droplet is given by:

$$m_p(t + \Delta t) = m_p(t) - N_i A_p M_{w,i} \Delta t \tag{3.23}$$

$M_{w,\,i}$ is the molecular weight, m_p is the droplet's mass, and A_p is the surface area of the droplet.

Finally, heat balance updates the droplet temperature, which helps the convective and latent heat transfer relate to the heat change in the droplet. This energy balance equation is given by:

$$m_p c_p \frac{dT_p}{dx} = hA_p\left(T_\infty - T_p\right) + \frac{dm_p}{dt} h_{fg} \tag{3.24}$$

In this equation, c_p and T_p are the heat capacity and temperature of the droplet. On the other side, h is the convective heat transfer coefficient, T_∞ is the gas phase temperature, h_{fg} is the latent heat.

3.3.3. Atomization

After the fluid is injected into the domain, the liquid film goes under atomization until the liquid is evaporated. The downstream is split into two sections depending on a particular phase's droplet size and volume fraction. Due to aerodynamic forces, the liquid

sheet is initially transformed into a tiny droplet (primary atomization) in the dense section.

Further, they are either disintegrated into smaller droplets or directly evaporated depending upon the droplet size after a primary breakup. This disintegration or the secondary atomization in a cryogenic spray is due to the kinetic energy of the primary breakup droplets or thermodynamic flashing. This flashing interaction occurs mainly due to the significant temperature difference between the fluid and the surrounding temperature. In this region, the collision of the droplets is the primary point of study as it

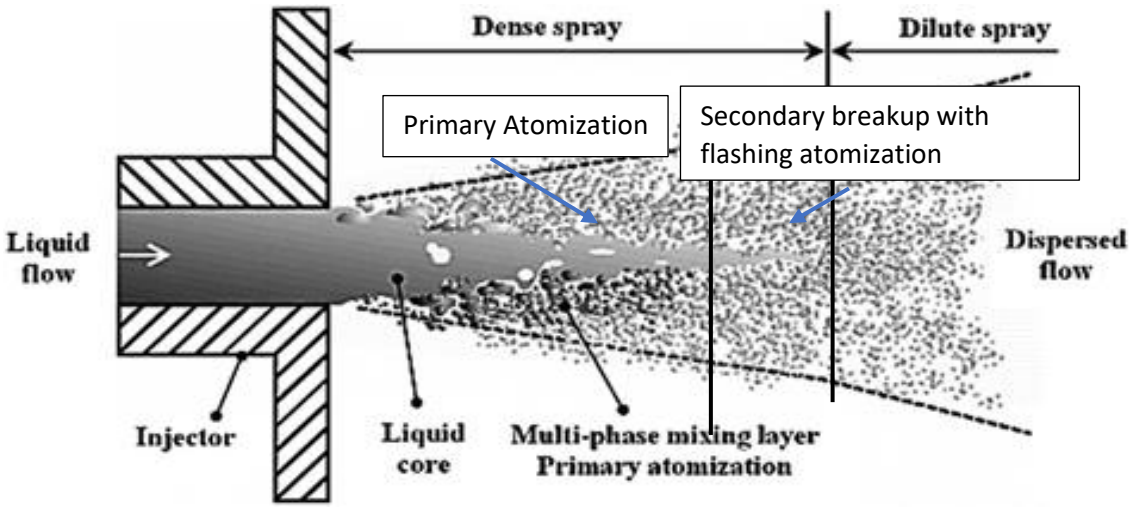

Figure 3.1 Sections of the spray formation (Paciaroni & Linne, 2013) (Modified)

cannot be neglected. The atomization and the collision mainly occur in the first section, i.e., in the dense region.

As the volume fraction of the droplet is high enough, there might be a random collision that can further merge to form a high viscous droplet, known as coalescence. In

further downstream or the diluted spray, the kinetic energy of the dispersed phase is so minute that the collision of the droplet can be overlooked.

3.3.4. Primary Breakup

The initial primary atomization mostly depends on the type of nozzle. Ansys Fluent provides a variety of different models for various nozzle types. For example, the pressure swirl atomizer is widely used in the cryogenic spray industry. The transition from internal injector flow to fully developed occurs in three stages: film formation, sheet breakup, and atomization. Ansys fluent uses the Linearized Instability Sheet Atomization (LISA) model of Schmidt et al. (1999) to model the nozzle for this atomizer.

The liquid sheet's primary breakup is considered to be due to aerodynamic instabilities. The secondary breakup, coalescence, or collision occur mainly after the droplet formation. Therefore, this model is divided into two stages: film formation and sheet breakup. The entire procedure for atomization is further explained in detail in Ansys Fluent Theory Guide 2021 (Ansys-Inc, 2009).

As the fluid exit the nozzle, a liquid film formation occurs, as shown in Figure 3.1. The thickness of this film can be computed using the simple fluid mechanics principle, mass flow rate equation:

$$\dot{m}_l = \pi \rho_l u h_o (d_o - h_o) \tag{3.25}$$

where ρ is the density of the fluid injected into the domain, h_o is the thickness of the film, u is the axial velocity, d_o is the injector exit diameter which depends on the nozzle type.

The total droplet rate can be estimated using injector pressure by:

$$U = k_v \sqrt{\frac{2\Delta p}{\rho_l}} \tag{3.26}$$

where k_v is the velocity coefficient which is the function of the injector pressure and its design. It can be calculated using:

$$k_v = max\left[0.7, \frac{4\dot{m}_{eff}}{d_0^2 \rho_l \cos\theta}\sqrt{\frac{\rho_l}{2\Delta p}}\right] \tag{3.27}$$

The thermodynamic property of the liquid phase is a function of temperature instead of pressure. The axial velocity required to find the mass flow rate can be determined using U as $u = U \sin\theta$. While the tangential velocity component is assumed to be the radial velocity component of the liquid sheet downstream of the injector exit: $\omega = U \sin\theta$ where θ is the spray angle

Once the sheet formation is completed, it moves forward to sheet breakup and atomization due to liquid viscosity, surrounding gas, and surface tension on the liquid sheet. The theoretical approach for this model was introduced by Senecal et al. (1999). This model requires two new unknown parameters: sheet constant and ligament constant. The former constant can be specified as Sheet constant = $ln\left(\frac{\eta_b}{\eta_0}\right)$ where η_b and η_o are the initial wave disturbance and surface disturbance at the time of the breakup.

Weber also obtained the sheet constant as 12 theoritically (Weber & Dresden, 1931), which was further confirmed by Dombrowski and Hooper (1962) experimental sheet breakup for over the range of Weber number from 2 to 200. Moreover, the Weber number was assumed to be more than the critical Weber number = 27/16 during the derivation to predict the initial breakup accurately. Therefore, the ligament constant is considered to be 0.5 by default. The droplet diameter is calculated using the Rosin-

Rammler equation for spray distribution considering a dispersion angle of 6º and spread parameter of 3.5.

3.3.5. Secondary Breakup

Ansys Fluent provides six breakup models from which the primary four are Taylor Analogy Breakup (TAB) model, Wave model, Kelvin-Helmholtz Rayleigh-Taylor (KHRT) model, and Stochastic Secondary Droplet (SSD) model. Ansys fluent suggests the TAB model for the liquid having low-injection velocity and being sprayed into the atmosphere. As the fluid is considered to have a low-Weber number and the domain is expected to be at atmospheric conditions, the TAB model is turned on for secondary atomization of unsteady injection.

The TAB works on the Taylor analogy between an oscillating and distortion of the droplets and the spring-mass system. Therefore, the spring's restoring force, external force, and damping force can be related to the surface tension, droplet drag, and droplet viscosity, respectively, for the distorting and oscillating droplet.

The resulting equations of the TAB model govern these features and can be solved for any specific time. When the droplet oscillation increases beyond the critical value, the larger droplet breaks into the number of droplets.

$$N^{n+1} = N^{n}\left(\frac{r^{n}}{r^{n+1}}\right)^{3} \tag{3.28}$$

The spring-mass system does not accurately describe the large shattering of the droplet due to the high Weber number. However, during the simulations low-Weber number is taken into consideration as it won't affect the accuracy of the simulation. As a result TAB was used to measure droplet breakup for higher accuracy and stability.

3.3.6. Coupling

The discrete phase equations can be solved based on the continuous phase flow field. This shows an uncoupled or a one-way approach. In the two-way coupled system, the discrete phase flow is affected by the ongoing phase flow, making it essential to reach the equilibrium between two fluid states. It is mainly considered for heat, mass, and momentum.

The continuous phase calculation considers the change in heat, mass, and momentum of the particle stream. The under-relaxation factor is introduced to improve the stability of the solution with increasing computational cost. The default value for under-relaxation factor α is 0.5, which can be reduced to improve strength.

The source terms are re-updated using the under relaxation factor by applying the following equation for mass, momentum, and energy represented by M, F, and Q, respectively. This conservation parameters can be updated using the Equations 3.29a-3.29c which considers the under relaxation factor (α) (Ansys-Inc, 2009).

$$M_{new} = M_{old}\alpha(M_{calculated} - M_{old}) \tag{3.29a}$$

$$F_{new} = F_{old}\alpha(F_{calculated} - F_{old}) \tag{3.29b}$$

$$Q_{new} = Q_{old}\alpha(Q_{calculated} - Q_{old}) \tag{3.29c}$$

Two methods can do the procedure of solving new particle source terms for a two-phase flow. The first method, also known as one-way coupling, includes solving discrete phase equations between gas and liquid phases based on the current gas-phase flow field. The gas-phase only affects the liquid phase in one-way coupling.

Moreover, in the second method, both the stages start affecting each other, known as two-way coupling. It includes solving the discrete phase equation using one-way coupling and then updating the source terms based on the discrete phase results and under relaxation factor using the Equations (3.29a-3.29c). This source terms of the discrete phase equations are solved till it converges.

4. Simulation Details

The main aim is to investigate the behavior of the cryogenic spray particles through particle tracking using the Lagrangian method. For this purpose, the experimental study by Rong X., et al. (2018) is used as a framework for our geometry and boundary condition. The structure for this study is summarized in the following sections.

4.1. Configuration

This section explains the detailed information about the geometry and meshing used during numerical simulation. The prime concern was to model the geometry based on the experimental setup (Xue, et al., 2018); however, if the experimental study failed to provide information then the standard assumptions or the data that best fitted the experimental results were taken into consideration.

4.1.1. Experimental Parameters

A schematic view of the cryogenic spray setup used during experimental analysis (Xue, et al., 2018) is shown in Figure 4.2. The system consists of six parts: the liquid nitrogen supply system, mass flow rate measuring system, subcooled system, spraying system optical measuring system, and finally, data acquisition system. As shown in Figure 4.2, once the liquid nitrogen is subcooled into the cryogenic temperature, it enters the spraying system, further injected into the atmosphere. The experiment is instrumented with an optical measuring system like a particle size analyzer, LED cold light source, and High-speed camera. The spraying system uses two nozzles with different outlet diameters: the plain orifice atomizer and the pressure swirl atomizer.

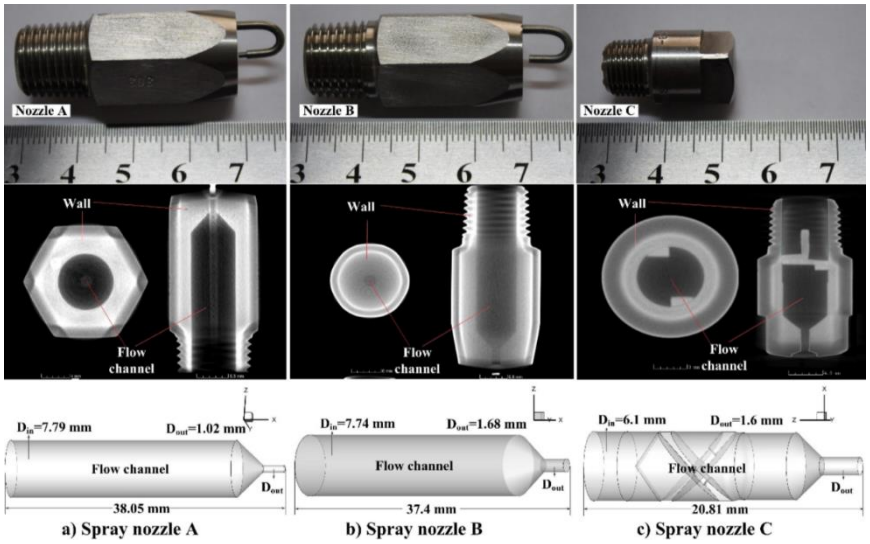

Figure 4.1 Nozzle measurements (Xue, et al., 2018)

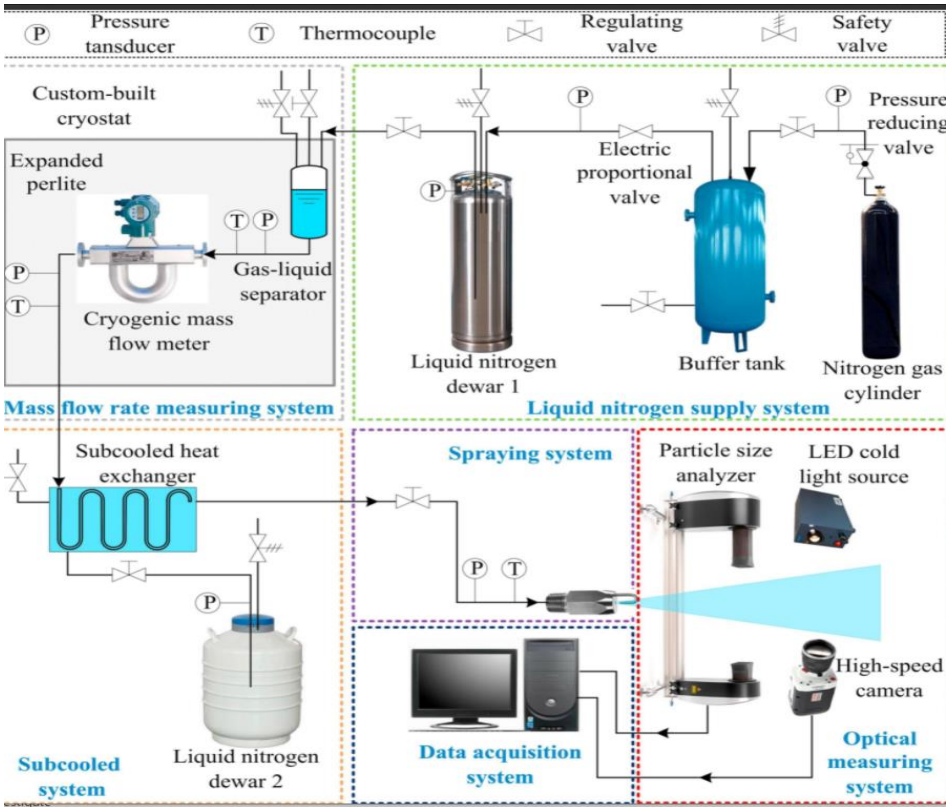

Figure 4.2 Schematic of the experimental setup for cryogenic spray (Xue, et al., 2018)

The detailed information of the design and dimension of the nozzle used during this experiment are described in Figure 4.1. In our simulation, nozzle B is preferred over nozzle A due to its simplicity. In this experiment, they obtained results for Sauter Means Diameter and spray cone angle.

4.1.2. Geometry and Grid Generation

The geometry and post-processing were carried out using SpaceClaim and Ansys post-processing. The geometry for numerical simulation was based on the experimental setup for plain pressure orifice; however, some parameters were deemed to be based on standard conditions to operate smoothly and with low computational cost. The geometry used in our simulation is shown in Figure 4.3.

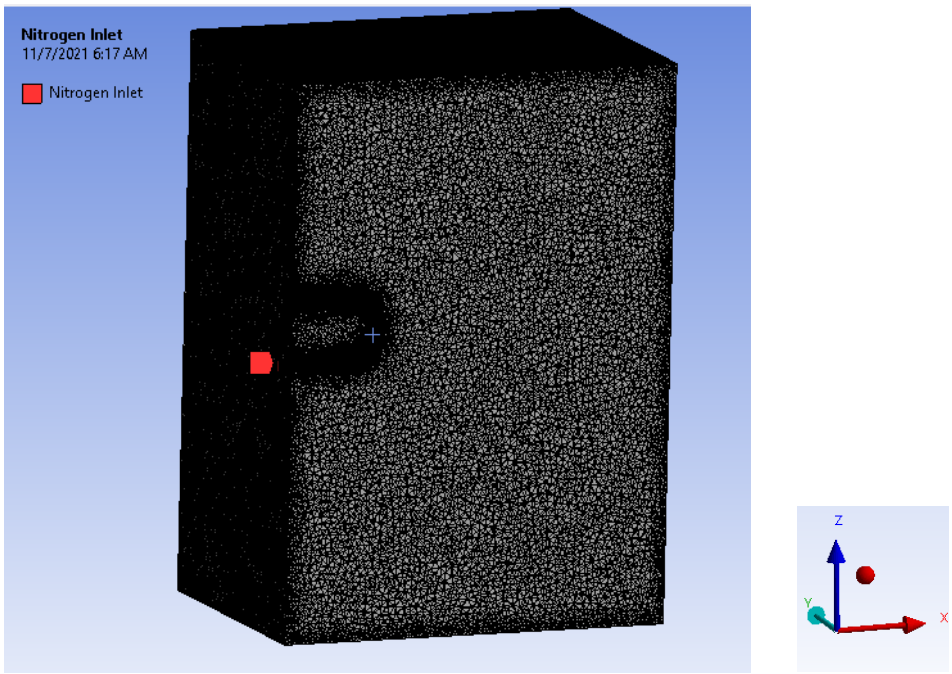

Figure 4.3 Geometry and grid (default) for simulation

For our simulation, the nozzle exit diameter was 1.68 mm. The fluid parameters were calculated and were used directly at the nozzle exit area during the simulation to reduce the computational costs. The control volume is a rectangular prism with a 70*70*50 mm^2 dimension having a uniform unstructured grid.

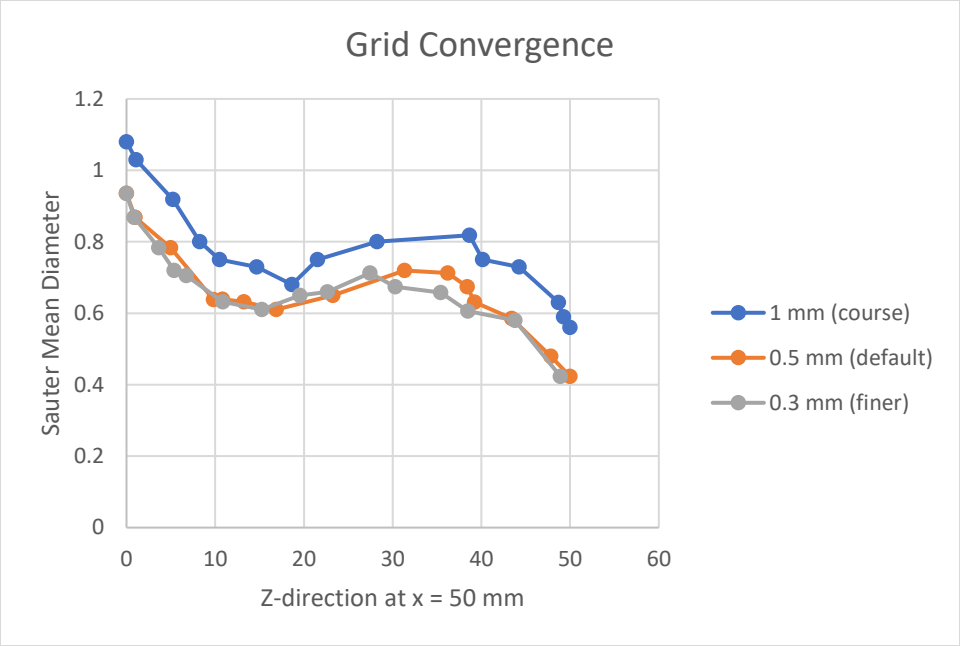

Figure 4.4 Grid Convergence

Three different element size grids is taken into consideration to verify the grid independence. The basis of this verification was the average maximum Sauter Mean Diameter (SMD) for pressure difference Δp = 0.2 MPa. Three unstructured meshes of approximately one, three, and seven million cells for 1mm (course), 0.5mm (default), and 0.3mm (finer) cell size, respectively, were taken into consideration. The results in Figure 4.4 show that the default grid is converged.

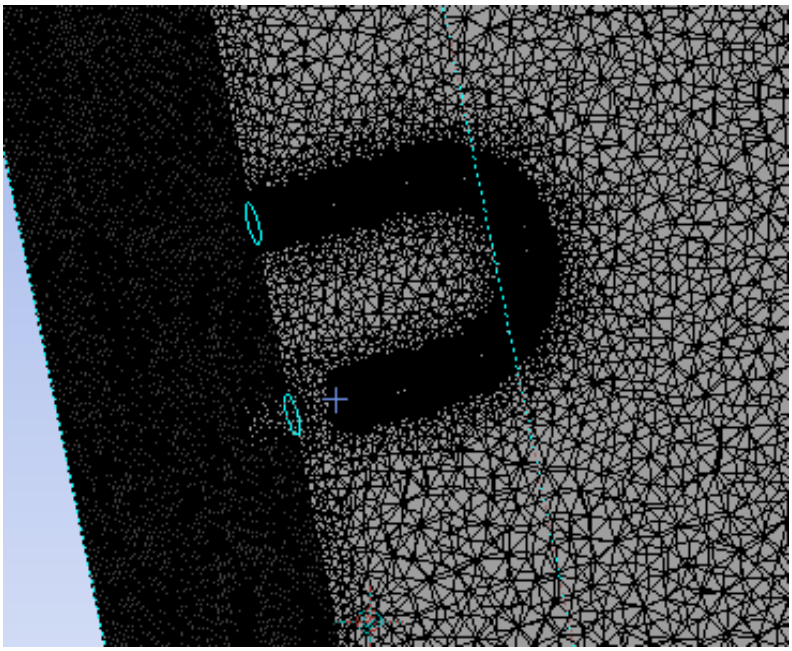

Figure 4.5 Grid near the pin

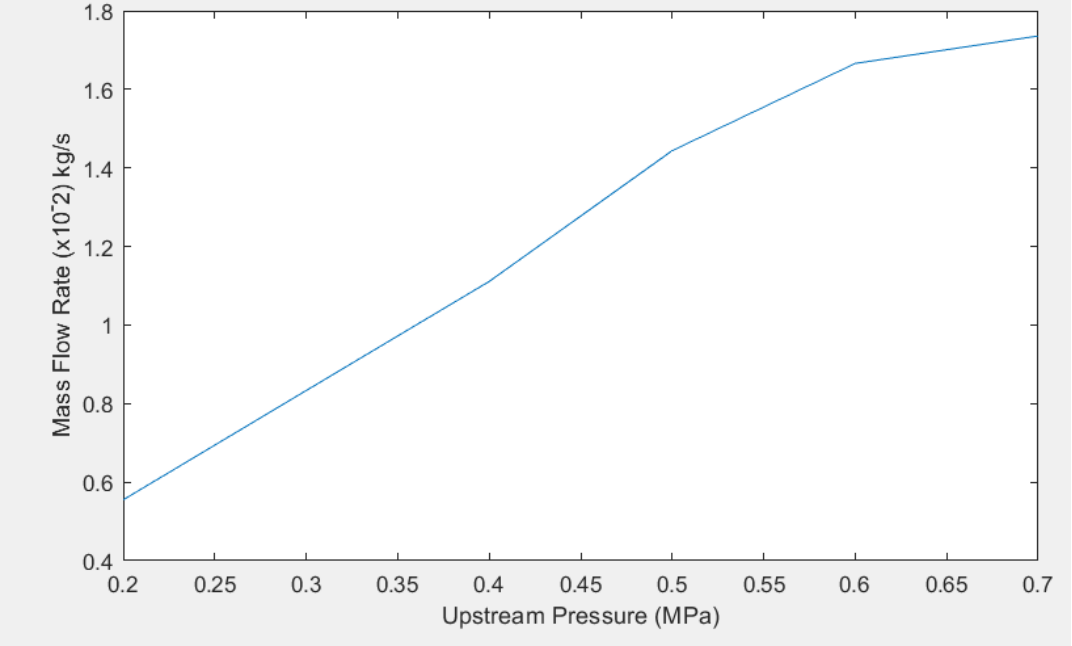

Figure 4.6 Pressure distribution along the mass flow rate

The default mesh was taken into consideration due to the comparatively high accuracy and lower computational cost. The liquid nitrogen strikes the pin to atomize further. So, mesh refinement is applied around the hook to capture a better boundary layer. Moreover, improving the entire mesh would be unnecessary, and it would instead increase the computational cost. This refinement of the mesh near the hook is shown in Figure 4.5.

The spray was injected into the domain with various upstream pressure with a controlled mass flow rate. It was varied according to the experimental study (Xue, et al., 2018), as shown in Figure 4.6. The pressure difference ranged from 0.2 MPa to 0.7 MPa with a constant atmospheric pressure of 101,325 Pa for a plain pressure orifice. Table 1 summarizes the unit of conditions pressure.

Liquid nitrogen was injected at 78 K, below its vaporization temperature for all the pressure differences. The physical time simulated is around 120 ms, as it provides the fully developed spray after injection and provides better correspondence with experimental results.

Table 4.1

Pressure Distribution for corresponding mass flow rate

Pressure (Pa)	Atmospheric Pressure	Pressure Difference (MPa)	Mass Flow rate ($x10^{-2}$ kg/s)
201,325	101,325 Pa	0.1	0.699
301,325		0.2	1.111
401,325		0.3	1.388
501,325		0.4	1.805
601,325		0.5	1.944
701,325		0.6	2.166

(Xue, et al., 2018)

4.2. Correspondance with Experimental Results

The experimental study of liquid nitrogen in the atmosphere (Xue, et al., 2018) has provided very few results. The main output generated during experiments were spray fields, spray cone angle, and the Sauter Mean Diameter of the particle.

The Sauter Mean diameter results produced during experiments are shown below in Figure 4.7. The condition applied to the numerical simulation were reproduced as of experimental study. During the experiment, the liquid nitrogen was sprayed into the atmosphere containing a handful amount of humidity. The droplet size was measured using a particle size analyzer, as shown in Figure 4.2. The particle size analyzer measures the size of any droplet using the laser diffraction technique.

Due to subcooled temperatures of liquid nitrogen, the moisture condenses to form water droplets along with the droplets of liquid nitrogen. So, the particle size analyzer measured the size of all the droplets, including condensed water present in the domain.

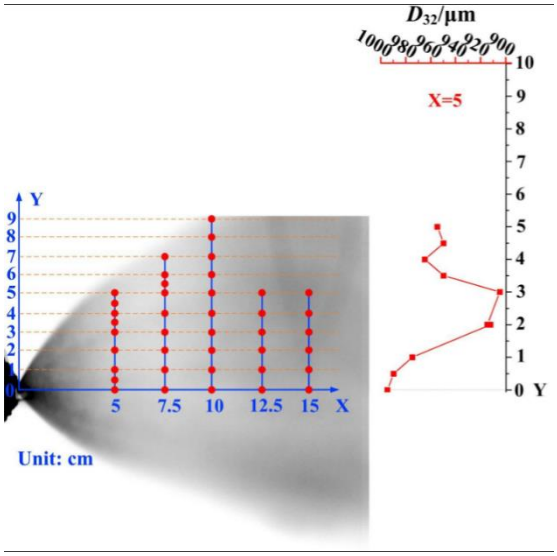

Figure 4.7 D_{32} using experimental analysis at Δp = 0.3 MPa (Xue, et al., 2018)

Figure 4.8 shows the spatial distribution of spray droplet diameter along the Y-direction at x = 50 mm. The range of droplet is found to be between 0.9 to 1 mm.

Moreover, during the numerical simulation, the liquid nitrogen was sprayed into the atmosphere for further atomization. Therefore, the results account for only nitrogen droplets throughout the domain. The diameter of the liquid nitrogen droplets was found to be between 0.4 to 1 mm. The range of the droplet diameter was found to be less than the experimental result, as water droplets were not considered during the simulations.

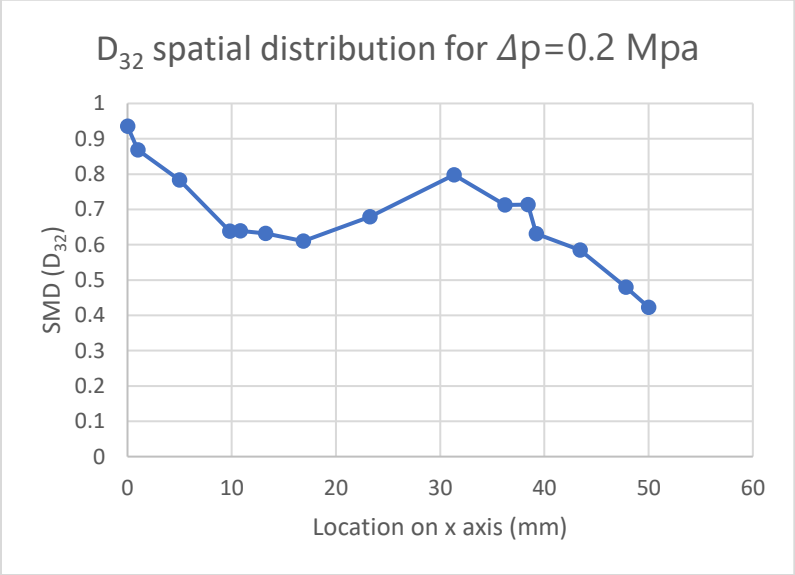

Figure 4.8 D_{32} using numerical analysis at Δp = 0.2 MPa

5. Results and Discussion

In this chapter, the results of various parameters are presented under the influence of pressure differences in the control volume. The liquid nitrogen is injected into the atmosphere at different injection pressure ranging from 201,325 Pa to 701,325 Pa. This pressure difference assists in understanding the evaporation effect with thermodynamic flashing and mechanical instability. This is similar to the experimental setup, where injection pressure is varied with reasonable mass flow rate and temperature.

5.1. DPM Sauter Mean Diameter

The contours of space-dependent DPM Sauter Mean Diameter (SMD) of liquid nitrogen for pressure difference 0.2 MPa are presented in Figure 5.1. Initially, liquid nitrogen is injected into the domain, which tends to disintegrate into tiny discrete particles. As the liquid nitrogen is injected at an 0^{o} angle, more droplets are concentrated along the center line of the flow. This results in a more significant droplet concentration around the center on spray flow. The droplets also tend to spread out into the domain due to pressure difference and the dispersion angle, forming a spray cone. This spread of liquid nitrogen contains a low droplet mass concentration. So, the droplet diameter near the circumference of the spray is reduced. However, due to the pin in front of the nozzle exit, the concentration and size of the droplet particle won't be symmetric along the centerline. Due to this pin, it is found that droplet diameter is less on the upper area of the nozzle exit compared to the lower side.

The SMDs are evaluated to analyze the atomization and the characteristics of the spray with non-uniform drop size. In Figure 5.1, the radial direction is defined as the y-

axis, while the axial direction of the spray flow is indicated along the x-axis.

Moreover, there is a very minute change in the average diameter downstream. This is due to evaporation flashing and coalescence occurring simultaneously. Therefore, a high amount of evaporation rate is present in the red circle, as shown in Figure 5.1, which is explained in the later section. Also, the kinetic energy of the gaseous nitrogen is transferred into the slow-moving liquid nitrogen droplet resulting in the collision of droplets, known as coalescence.

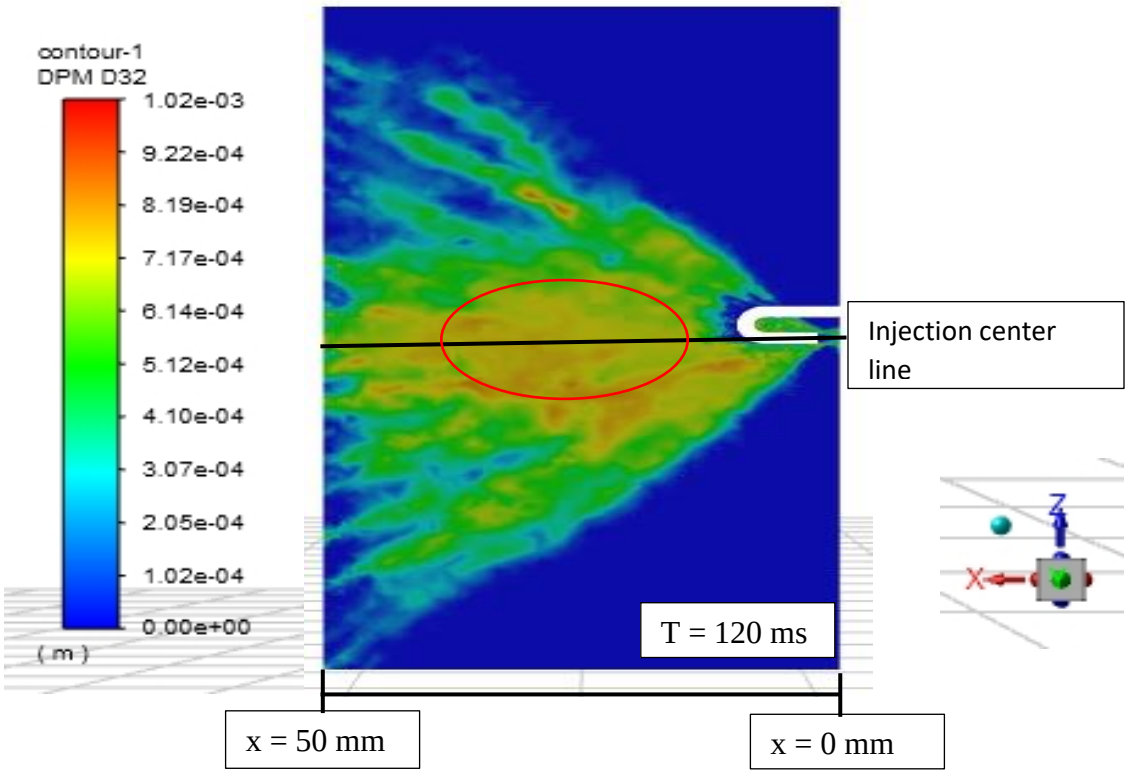

Figure 5.1 D_{32} Spatial Distribution for Δp = 0.2 MPa

There are also effects of pressure difference on the D_{32} of the spray formation, which is described in Figure 5.2. A target plane is considered at 50 mm in the axial direction of the spray as a reference. In that case, it is observed that the D_{32} for the spray decreases

with an increase in pressure difference. As the upstream pressure increases, the velocity of the downstream particle increases. This change in speed increases the atomization resulting in smaller droplets.

The z-direction in Figure 5.2 starts from the center line of the spray region. It also shows the maximum droplet diameter for a given pressure difference.

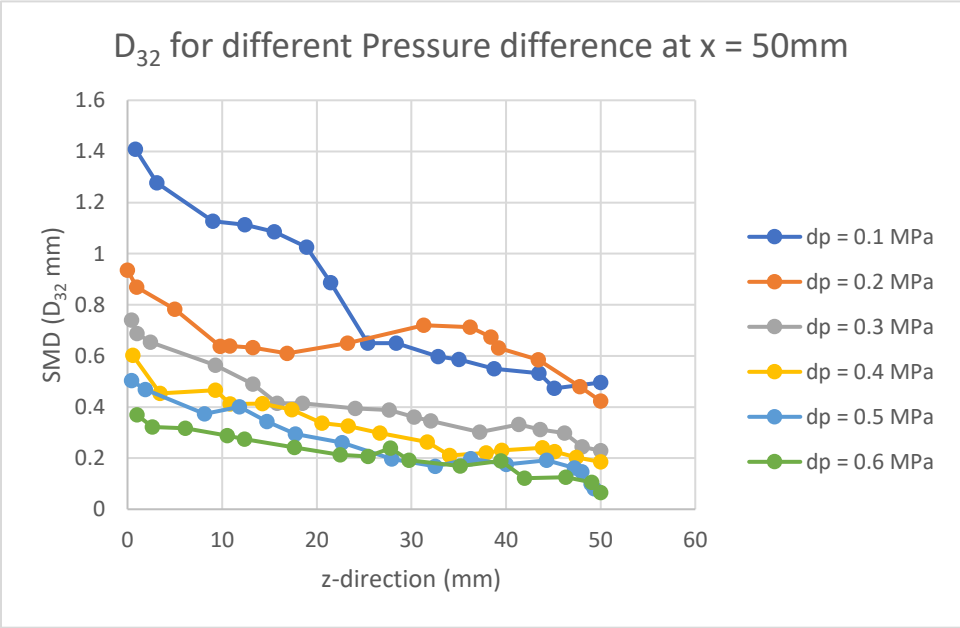

Figure 5.2 D_{32} for various pressure difference

The droplet diameter is further reduced as it moves near the boundaries of the spray cone. Figure 5.2 is the distribution of the droplet diameter at x = 50 mm. As particle has scattered over the region, the particle diameter keeps reducing as it moves away from the center (x = 0 mm). The DPM version of the spray at time 120 ms is shown in Figure 5.3 for the whole 3-D domain.

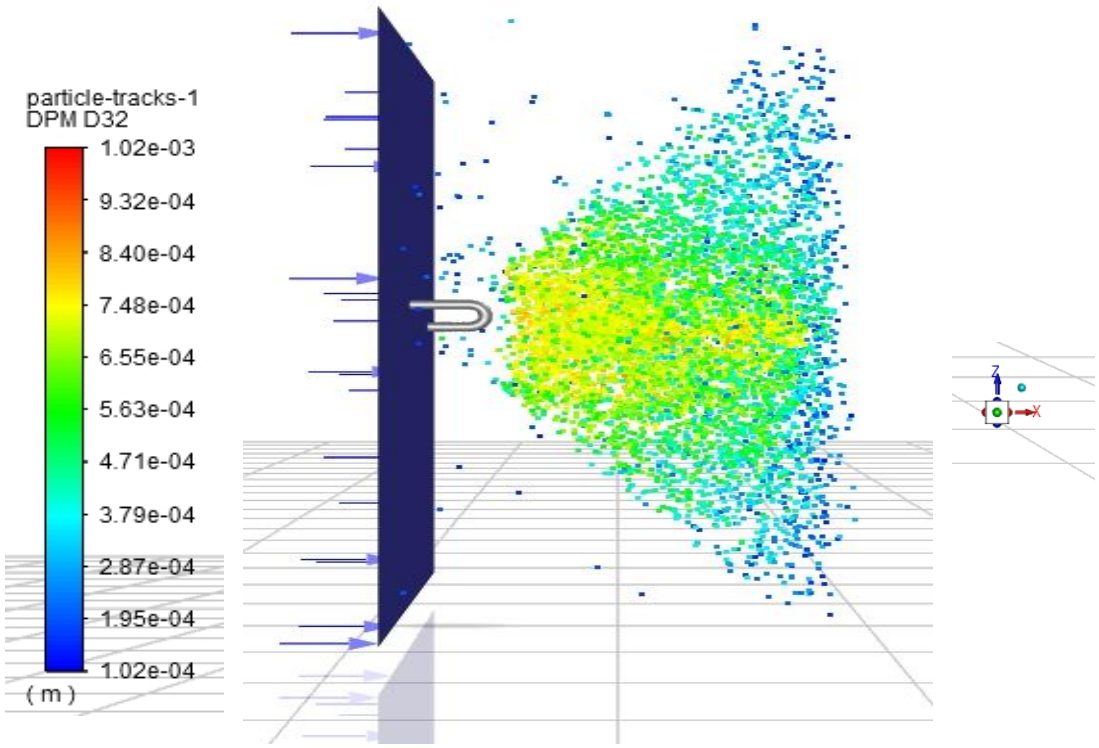

Figure 5.3 DPM distribution for Δp = 0.2 MPa

5.2. Evaporation Rate

The evaporation rates are presented in Figure 5.4. This Figure is along the center line at a given time. The trend for this evaporation can be divided into two parts. During the initial stage of the liquid nitrogen spray, the evaporation rate increases gradually to 15 mm in the axial direction. This change was during the primary breakup of the jet.

As the mist moves further downstream, there is an exponential rise in the evaporation rate near the nozzle exit. This increase in evaporation rates can occur mainly due to secondary breakup and thermodynamic instability during a secondary separation. The secondary atomization causes a droplet to disintegrate, resulting in smaller particles. As the ratio of volume to the surface area becomes smaller, the evaporation rate increases.

However, there is a steep rise in the evaporation rate, which is generally not only due to secondary breakup. This gives rise to another irregularity in the domain which also drives the evaporation rate. The cryogenic spray has some uncertainty, mainly caused by the significant temperature difference between the atmosphere and the vaporization temperature of the fluid. It can be defined as thermodynamic flashing or flashing instability.

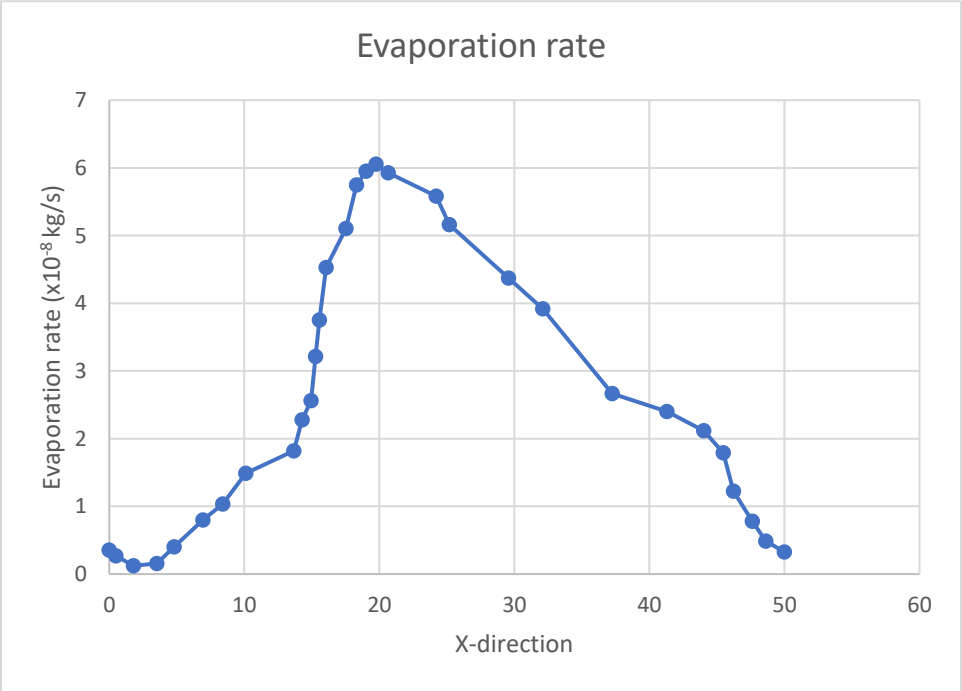

Figure 5.4 Evaporation rate for Δp = 0.2 MPa

Moreover, the evaporation rate gradually starts decreasing once the peak is achieved. During this area, the maximum amount of liquid has been evaporated. However, incomplete evaporation is still occurring due to Turbulent Kinetic Energy present in the environment, further discussed in the DPM velocity section. This energy forces droplets

to move further, delaying the evaporation rate. This momentum of the droplet creates a gradual decrease in the evaporation rate.

A small amount of evaporation is also observed near the edge of the spray cone. There is a minimum amount of evaporation far away from the axial center of the spray along the z-direction.

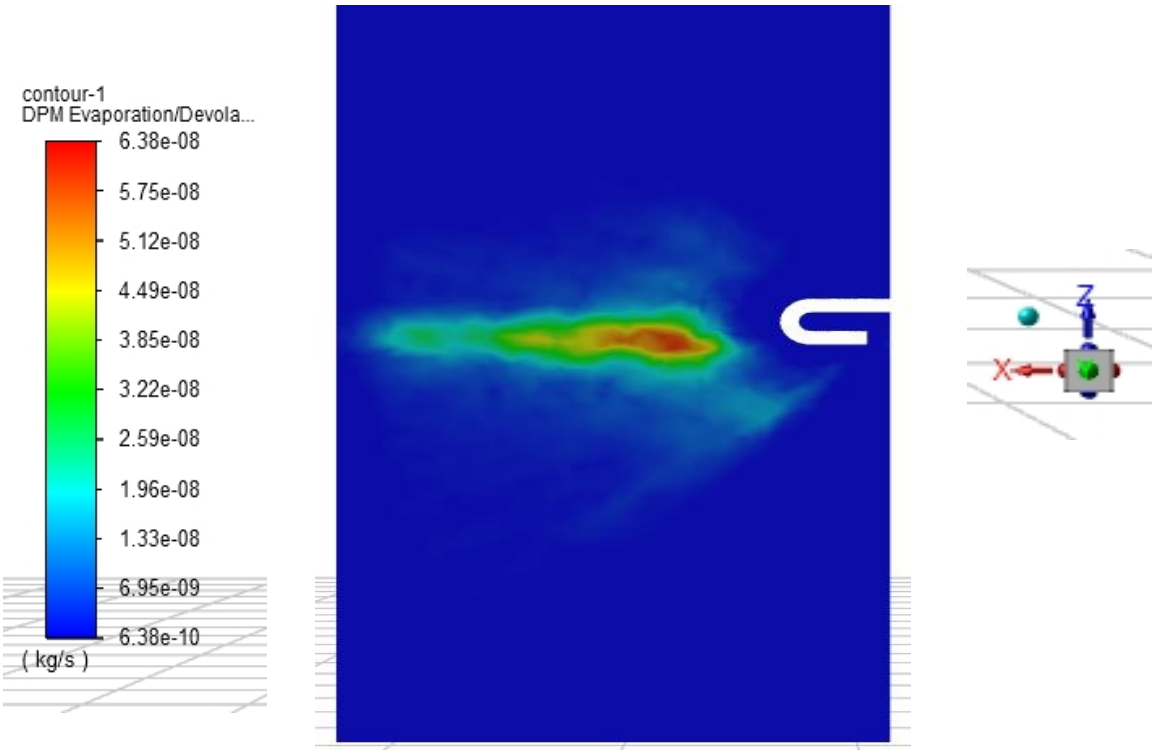

Figure 5.5 Contour plot for evaporation rate for Δp = 0.2 MPa

This evaporation is due to the smaller droplet size in that area. Moreover, the evaporation rate is increased along with the pressure difference and the mass flow rate. As the mass flow rate increases, the particle in the domain also increases, showing an uptrend in evaporation rate. This variation is clearly shown in Figure 5.6.

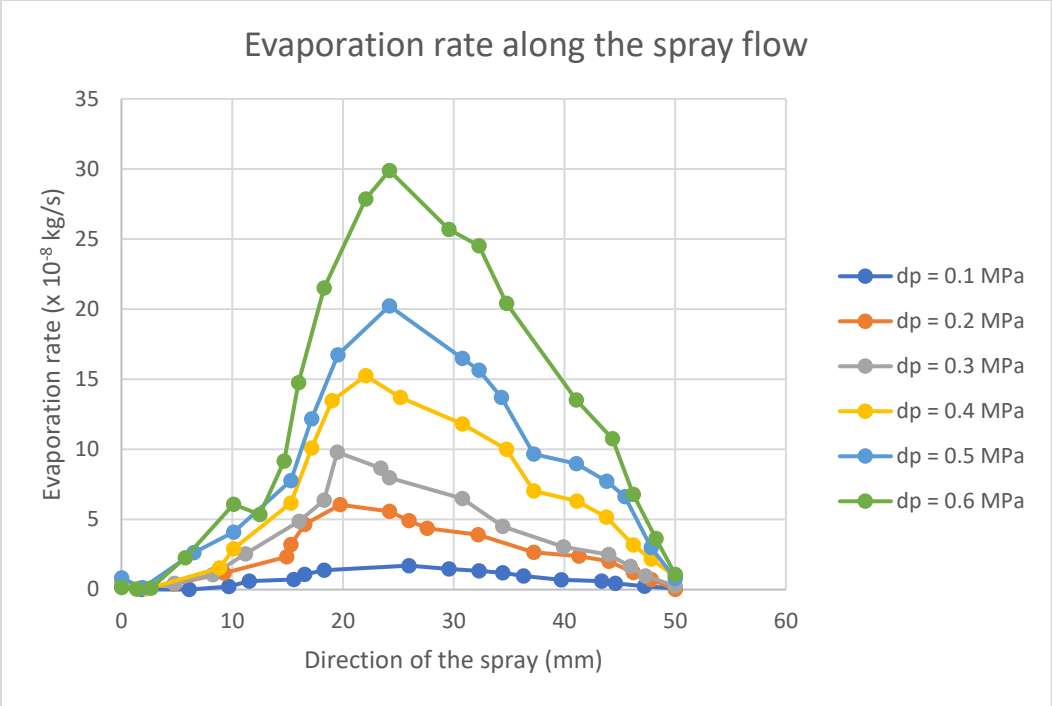

Figure 5.6 Evaporation rate along the spray flow at different pressure difference

5.3. Spray Cone Angle

The angle between two spray boundaries at 20 mm from the nozzle exit is considered a spray cone angle. This distance was selected based on the experimental data (Xue, et al., 2018). Thus, the spray field is almost covered by nitrogen vapor downstream of the acceptable mist nozzle outlet. The dispersion angle is set to be 100^{o} for all the pressure difference cases. The dispersion angle is measured according to the condition shown in Figure 5.7. The angle is set to be high for the fluid to have a straight flow into the domain.The spray cone angle was measured using the DPM concentration and CATIA V5 software at an axial distance of 20 mm from the nozzle exit.

The spray cone angle was smaller than the dispersion angle because of the environmental condition like pressure difference between the surrounding and liquid nitrogen spray, and other physical parameters like nozzle exit diameter, type of nozzle, and the distance between the nozzle exit the pin. The variation of spray cone angle for different upstream pressure is shown in Figure 5.7, along with the dispersion angle. Moreover, as the upstream pressure increases, the far-field spray tends to shrink. However, the distance between the nozzle exits and the pin's tip is kept constant for all the cases. The experimental data for this simulation condition is shown in Figure 5.8 in blue color.

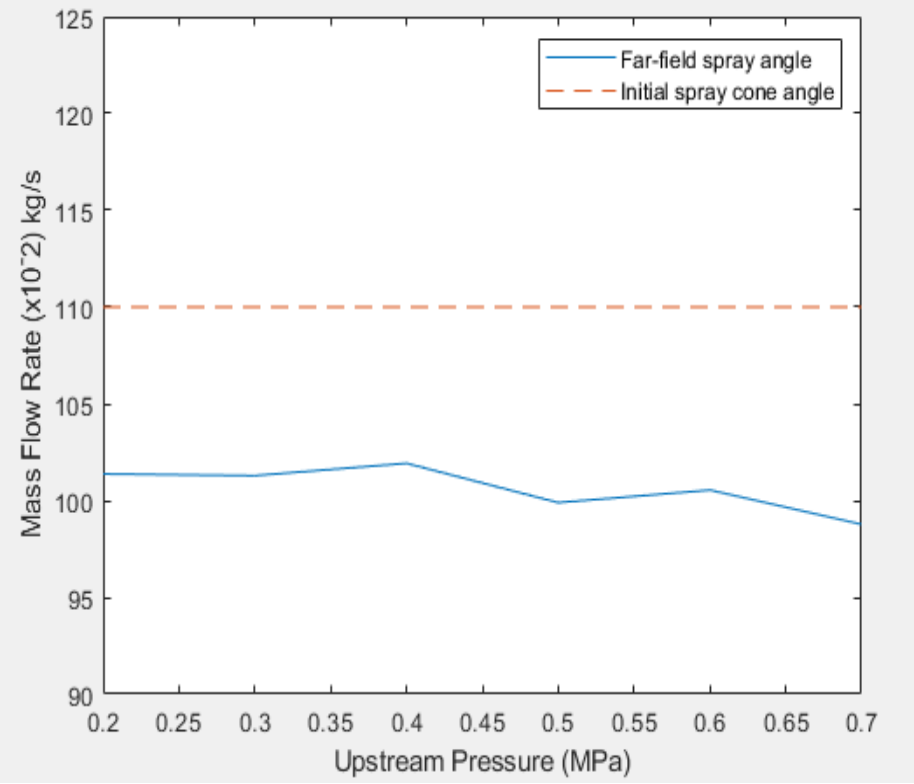

Figure 5.7 Far-field angle w.r.t. Initial spray angle

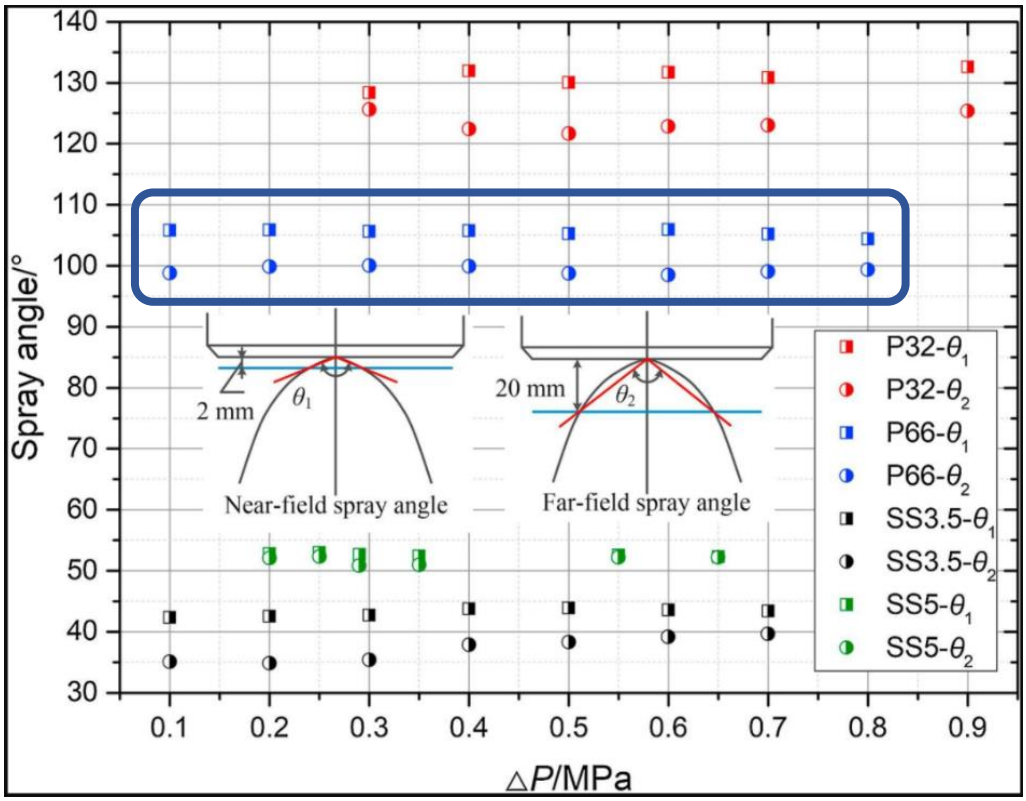

Figure 5.8 Experimental data for spray cone angle *(Xue, et al., 2018)*

5.4. DPM Density

In the test case, liquid nitrogen was injected into the environment at 78 K temperature with the variable upstream pressure. The density for liquid nitrogen was considered as 816 kg/m^3 for the given temperature. Figure 5.9 shows the density distribution in the computational domain for various pressure differences. The density was found to be close to that of liquid nitrogen in the center of the spray indicating, it can be predicted that the concentration of LN_2 is high in that region as the density of gaseous nitrogen is around 1.068 kg/m^3. The area not covered by the spray cone has a density of 1.225 kg/m^{3,} indicating the presence of atmospheric air.

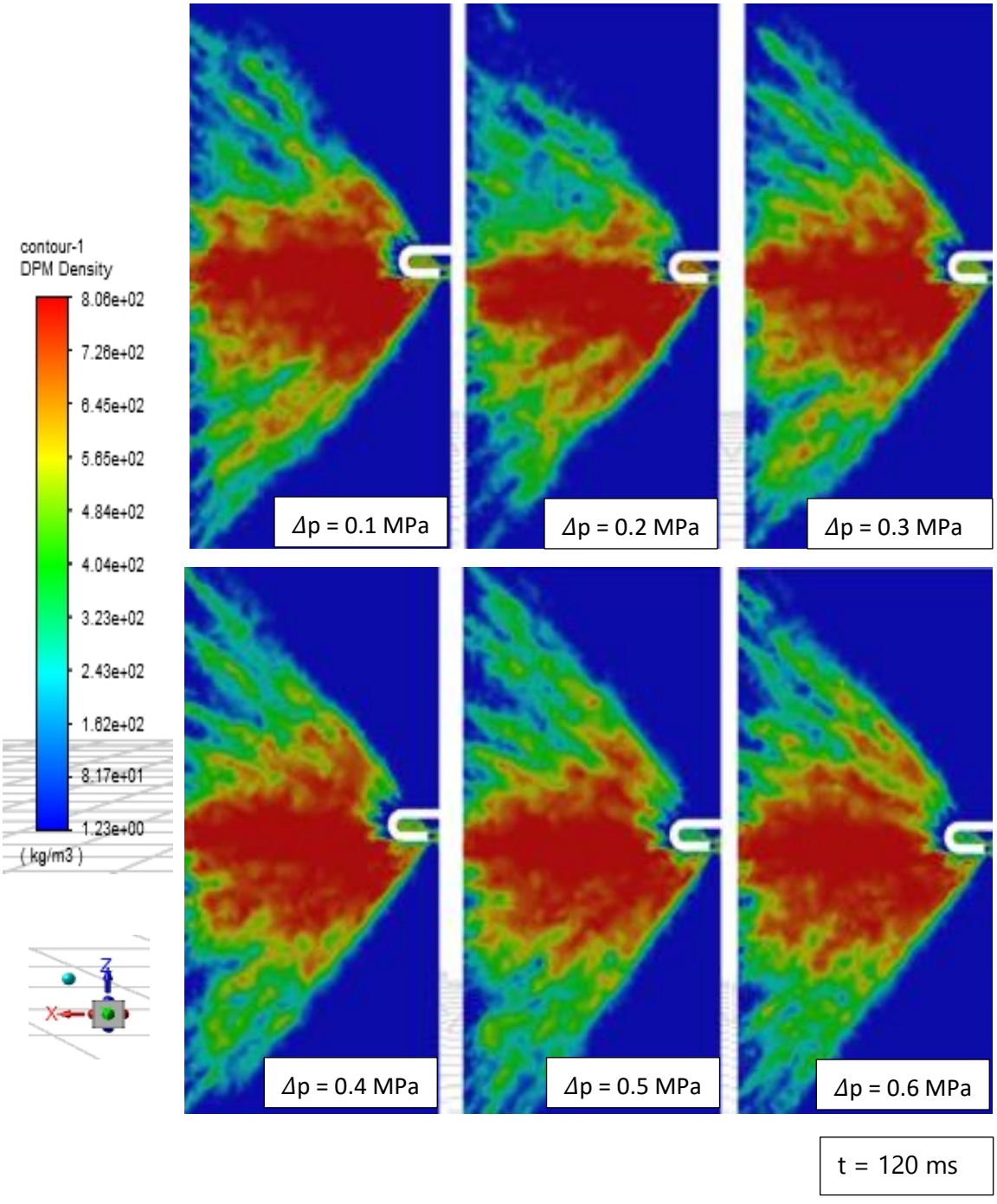

Figure 5.9 Density distribution of liquid nitrogen at the center of the spray

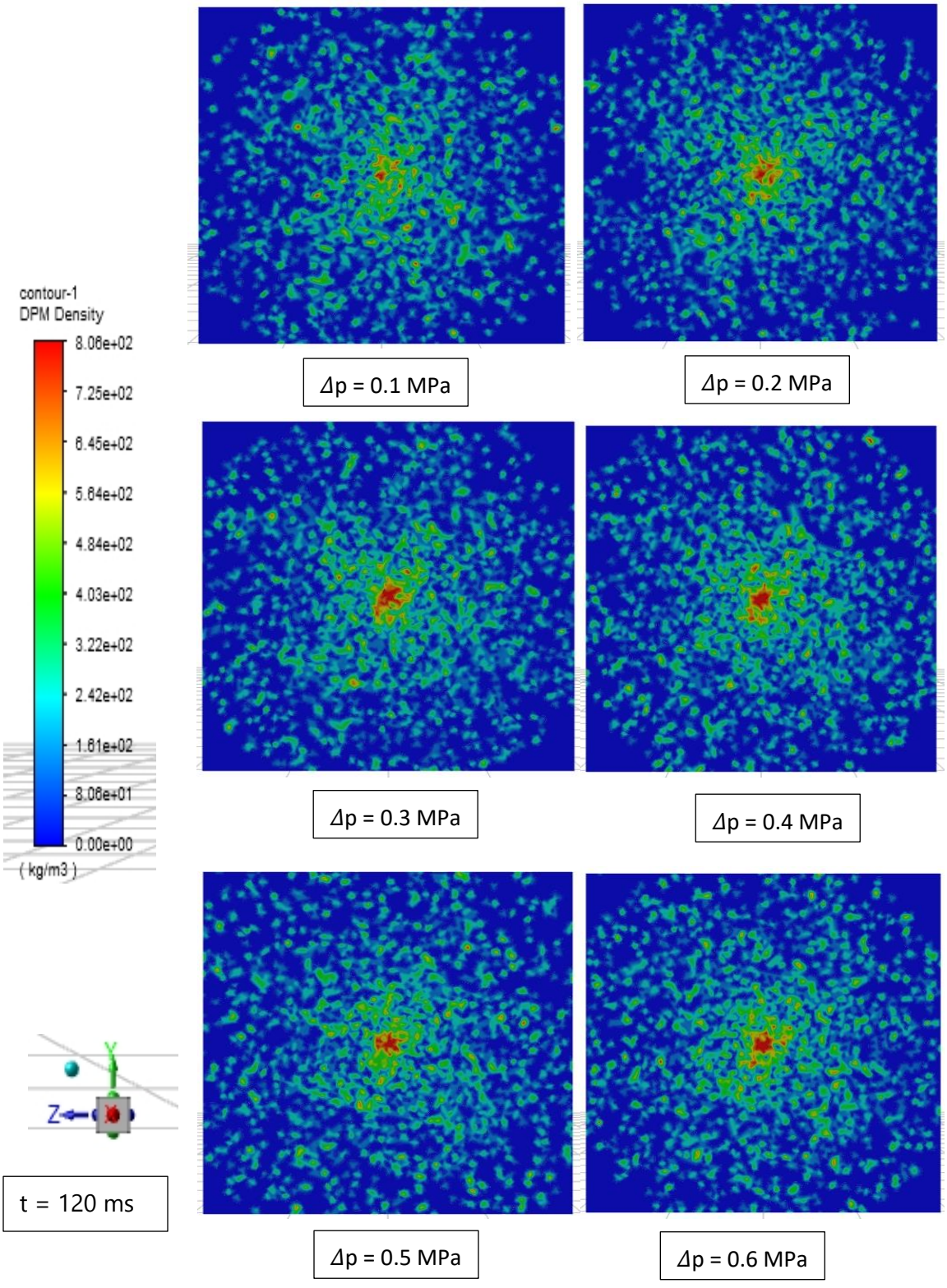

Figure 5.10 Density of liquid nitrogen over the target plate at 50 mm

However, there was a decrease in density near the outer edge of the spray cone due to the liquid droplet's transformation into the gaseous form. Next, the liquid nitrogen concentration increases with the increased pressure difference and mass flow rate for a given constant nozzle tip to the nozzle exit distance and the injection temperature. Figure 5.9 also shows the density of 806 kg/m^3 as the pressure difference increases along the center plane of the spray. The concept of a mass fraction is essential to understand as it helps to understand the effective cooling rate through liquid nitrogen over the target plate.

The target plate was set at 50 mm from the nozzle exit in the axial direction. Moreover, the concentration of liquid nitrogen increases in the center region of the targeted plate as the pressure difference rises as shown in Figure 5.10. The droplet tends to move faster due to the Turbulent kinetic energy, which increases the penetration length. This can result in more effective cooling.

The mass fraction of liquid nitrogen seems to change exponentially near the periphery of the spray due to smaller droplet distribution, low density, and less concentration of the particles.

5.5. Droplet Velocity

The distribution of droplet velocity over the domain for pressure difference Δp = 0.2 MPa is shown in Figure 5.11. This velocity distribution was measured on the plane parallel to the flow passing through the nozzle's center. The velocity peak is primarily recorded on the centerline of the spray in the axial direction. Furthermore, the axial velocity of the liquid droplet is also caused due to the momentum of the gaseous particle. This results in the acceleration of liquid nitrogen droplets in the domain within 20 mm from the nozzle exit.

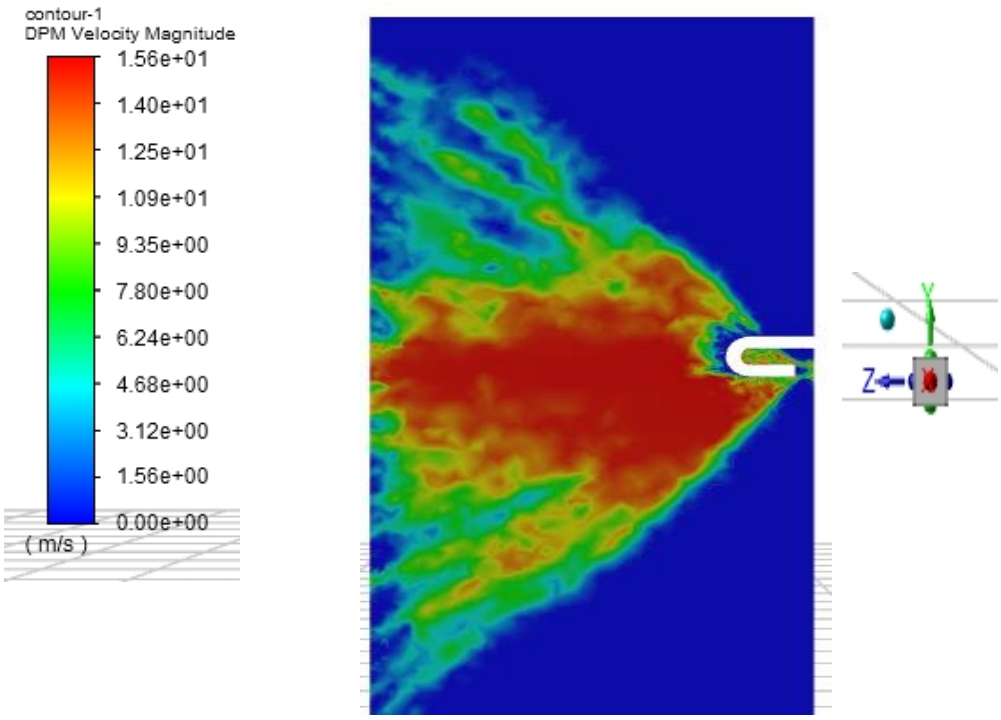

Figure 5.11 Velocity Contour for *Δ*p 0.2 MPa

The peak velocity was found as 15.5 m/s and further reduced gradually towards the downstream of the flow. This increase in the speed of the droplet gives rise to Turbulent Kinetic Energy, resulting in a high turbulent flow.

The velocity also reduces because tiny droplets near the periphery of the spray cone tend to evaporate faster as it move away from the axial centerline. This velocity rate change is clearly shown in Figure 5.11 as there is a sudden decrease of speed, i.e., from 7.8 m/s to around 1.56 m/s. In addition, due to the pin, it is observed that momentum in the upper phase of the spray flow has a comparatively lower speed than the bottom side over the whole spray cone region. This reduced the impact of liquid nitrogen on the upper area of the target.

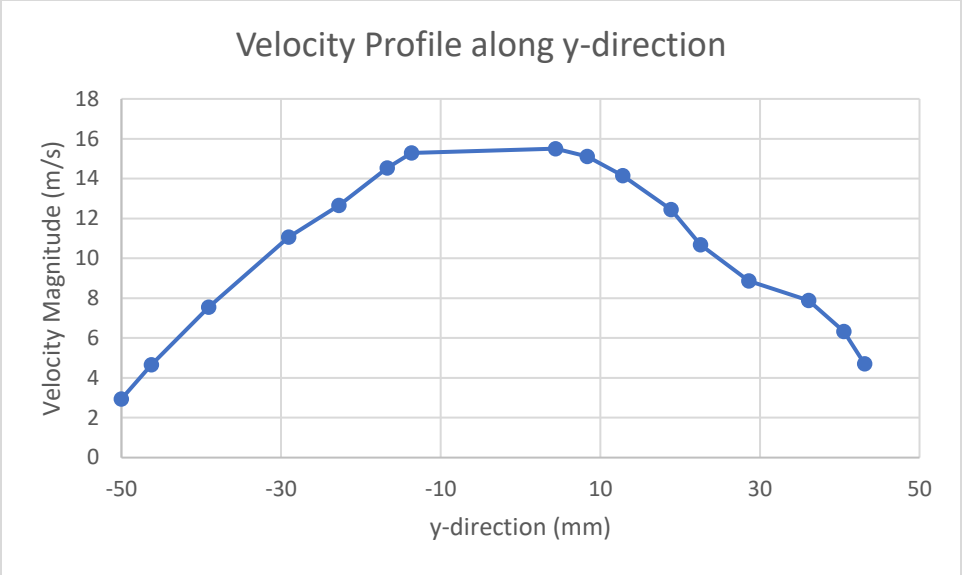

Figure 5.12 Velocity profile along y-direction

Figure 5.12 shows the maximum velocity profile along the y-direction on the center plane of the spray considering x = 0 mm and z = 50 mm spray at time = 120 ms. Due to the pin, there wasn't any particle having a velocity vector spotted near the upper region of the target plate.

As the pressure difference increases, this constant region of maximum velocity has shifted into positive y-direction, as shown in Figure 5.13. Assitionally, Figure 5.13 is a velocity profile of the spray cone for different pressure differences along the y-direction for given x = 0 and z = 50 mm (target plate). Moreover, the top speed of the droplets has also increased along with the upstream pressure. Due to the high-pressure difference, the injected mass flow rate has also increased in the domain, resulting in droplets on the corner of the target with at least minimal velocity.

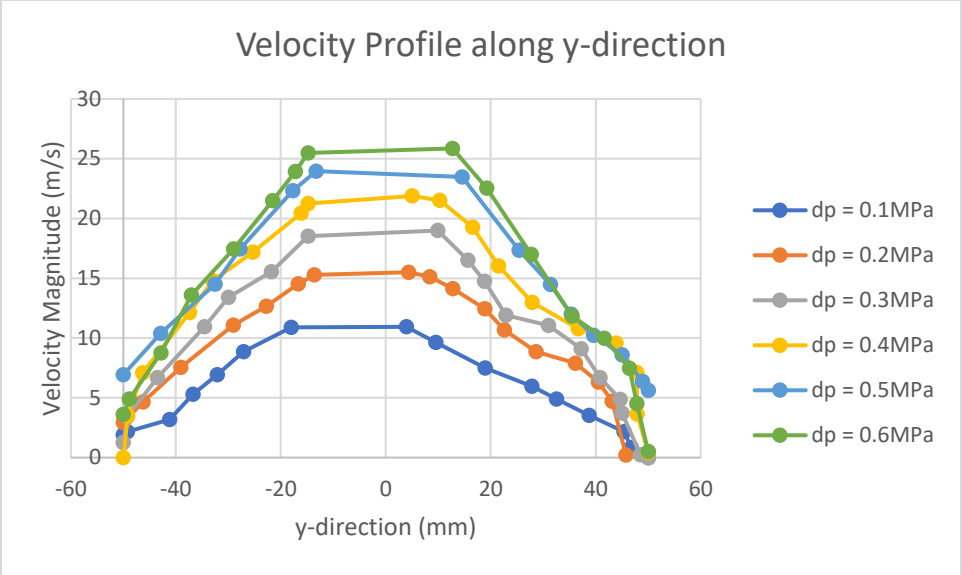

Figure 5.13 Maximum velocity for various pressure difference

Due to the increase in velocity profile, it can also be indicated that there is a high impact of liquid nitrogen over the target plate (z = 50 mm) which was not clearly shown by the experimental study.

6. Conclusion And Future Work

The numerical simulation were performed on cryogenic spray. These simulations were accomplished using Ansys Fluent 2021 and include many state of art models. The simulation was performed using an Euler-Lagrangian approach with a Discrete Phase Model (DPM). The flow Turbulent was modeled by k-omega equations incorporated with the shear stress transport (SST) model. The primary breakup was evaluated using the Linearized Instability Sheet Atomization (LISA) model. This model helped to simulate the breakup of a liquid sheet into the discrete particle. Furthermore, the secondary breakup of the particle was modeled using Taylor Analogy Breakup equations and merged with evaporation-condensation to evaluate the phase change in the domain.

Our study showed that the Sauter Mean Diameter (D_{32}) tends to increase toward the center of the spray on a plane perpendicular to the spray flow direction. The reduction in droplet diameter along the axial direction is due to the aerodynamic breakup, and the numerical data also showed thermodynamic instability. Moreover, the numerical simulation indicated the particle size had drastically reduced along the centerline once the upstream pressure increased. However, there was not much difference at the periphery of the target among the high pressure.

The droplet diameter clearly showed the distribution of the particle in the spray field. The droplets were spread across the domain for almost a large area in the environment forming around 95^{o} to 105^{o} spray cone angle. This angle did not significantly change for the high-pressure difference. In other words, it is found that the upstream pressure does not affect the spray cone angle substantially.

The simulation also showed a significant change in maximum evaporation rate while changing the upstream pressure. However, the pattern for the evaporation rate remains similar for all the cases.

The droplet density was used to infer the presence of liquid nitrogen and gaseous nitrogen in the domain. The numerical results demonstrated the concentration of liquid nitrogen is focused on the center of the spray and reduces as it moves near the border of the jet. It is also suggested that the increase in pressure injection is likely to cause the spray to hit the desired target with a more significant amount of liquid nitrogen. The liquid concentration increases over the plate, covering a larger area over plate. The spray pattern was found to be different for a specific position while adjusting the pressure.

The velocity is lower near the circumference of the spray as the droplet diameter is reduced. In addition, a significant effect of pressure on the velocity profile of the spray was found. So, the increase in pressure resultsin in velocity increase.

Finally, some suggestions for future work based on this study are below:

- New models should be tested with discrete phase models.
- More modern and accurate evaporation models like the Homogeneous relaxation model can be integrated with this model, as earlier studies have reported promising results.
- Isolated effects of the different models should be quantified in a suite of numerical experiments to further theoretical insights into the cryogenic spray phenomenon.

References

Aguilar, G., Majaron, B., Pope, K., Svaasand, l. O., Lavernia, E. J., & Nelson, J. S. (2001). Influence of nozzle-to-skin distance in cryogen spray cooling for dermatologic laser surgery. *Lasers Surg Med*, 113-120. doi:10.1002/lsm.1025

Ansys-Inc. (2009). *Ansys Fluent 12.0 User's Guide.* Canonsburg, CA: Ansys Inc.

Cader, T., Westra, L. J., & Eden, R. C. (2004). Spray cooling thermal management for increased device reliability. *IEEE Transactions on Device and Materials Reliability*, 605-613. doi:https://doi.org/10.1109/TDMR.2004.838978

Chang, M., Lee, Z., Park, S., & Park, S. (2020). Characteristics of flash boiling and its effects on spray behavior in gasoline direct injection injectors: A review. *Fuel*. doi:https://doi.org/10.1016/j.fuel.2020.117600

Chen, B., Wang, R., & Wang, X.-S. (2017). Numerical simulation of cryogen spray cooling by a three-dimensional hybrid vortex method. *Applied Thermal Engineering*, 319-330. doi:https://doi.org/10.1016/j.applthermaleng.2017.03.066

Chen, J., Gao, X., Bao, S., Hu, L., & Xie, J. (2020). Numerical analysis of spray characteristics with liquid nitrogen. *Cryogenics, 109*(103113). doi:https://doi.org/10.1016/j.cryogenics.2020.103113

Chen, J., Gao, X., Bao, S., Shao, S., Hu, H., Zhou, S., & Xie, J. (2020). Theoretical analysis on the atomization characteristics of liquid nitrogen jets. *Physics of Fluids, 32(5)*(54102). doi:https://doi.org/10.1063/5.0004820

Chen, R.-H., Chow, L. C., & Navedo, J. E. (2002). Effects of spray characteristics on critical heat flux in subcooled water spray cooling. *International Journal of Heat and Mass Transfer, 45(19)*, 4033-4043. doi:https://doi.org/10.1016/S0017-9310(02)00113-8

Chow, L. C., Sehmbey, M. S., Hahn, O. J., & Pais , M. R. (1995). Effect of Spray Characteristics on Spray Cooling with Liquid Nitrogen. *Journal of Thermophysics and Heat Transfer, 9(4)*, 757-765. doi:https://doi.org/10.2514/3.735

Cleary, V., Bowen, P., & Witlox, H. (2007). Flashing liquid jets and two-phase droplet dispersion: I. Experiments for derivation of droplet atomisation correlations. *Journal of Hazardous Materials, 142(3)*, 786-796. doi:https://doi.org/10.1016/j.jhazmat.2006.06.125

Dombrowski, N., & Hooper, P. C. (1962). The effect of ambient density on drop formation in sprays. *Chemical Engineering Science*, 291-305. doi:https://doi.org/10.1016/0009-2509(62)85008-8

Dress, D. A., & Kilgore, R. A. (1984). The application of cryogenics to high Reynolds number testing in wind tunnels. Part 1: Evolution, theory, and advantages. *Cryogenics, 24(8)*, 395-402. doi:https://doi.org/10.1016/0011-2275(84)90011-0

Ested, K. A., & Mudawar, I. (1995). Correlation of sauter mean diameter and critical heat flux for spray cooling of small surfaces. *International Journal of Heat and Mass Transfer, 38(16)*, 2985-2996. doi:https://doi.org/10.1016/0017-9310(95)00046-C

Fey, U., Engler, R. H., Egami, Y., Iijima, Y., Jansen, U., & Quest , J. (2003). Transition detection by temperature sensitive paint at cryogenic temperatures in the European Transonic Wind tunnel (ETW). *20th International Congress on Instrumentation in Aerospace Simulation Facilities. ICIASF '03.*, pp. 77-88. IEEE. doi:10.1109/ICIASF.2003.1274855.

Fung, M. C., Inthavong, K., Yang, W., Lappas, p., & Tu, J. (2013). External characteristics of unsteady spray atomization from a nasal spray device. *National Library of Medicine, 102(3)*, 1024-1035. doi:10.1002/jps.23449

Gao, X., & Li, R. (2018). *Spray Impingement Cooling: The State of the art.* IntechOpen.

Gartner, J. W., Kronenburg, A., Rees, A., Sender, J., Oschwald, M., & Lamanna, G. (2020). Numerical and experimental analysis of flashing cryogenic nitrogen. *International Journal of Multiphase Flow*, *130*(103360). doi:https://doi.org/10.1016/j.ijmultiphaseflow.2020.103360

Gimeno, J., Salvador, F. J., Pastor, J. M., & Marti-Aldaravi, P. (2014). Effect of turbulence model and inlet boundary condition on the Diesel spray behavior simulated by an Eulerian Spray Atomization (ESA) model. *International Journal of Multiphase Flow, 65*, 108-116. doi:https://doi.org/10.1016/j.ijmultiphaseflow.2014.06.003

Hanson, E. (2020). Experimental Investigation of Prestigation of a Pressure-Swirl Atomizer Spray. *RIT Scholar works*, 1095-1101. doi:https://doi.org/10.2514/1.28513

Holyst, R., Litniewski, M., Jakubczyk , D., Kolwas, M., Kowalshi , K., Migacz , S., . . . Zientara , M. (2013). Evaporation of freely suspended single droplets: Experimental, theoretical and computational simulations. *Reports on progress in physics, 76(3)*, 76,3. doi:10.1088/0034-4885/76/3/034601

Hou, Y., Liu, J., Su, X., Qian, Y., Liu, L., & Liu, X. (2014). Experimental Study on the Characteristics of a Closed Loop R134-a Spray Cooling. *Experimental Thermal and Fluid Science, 61*, 194-200. doi:https://doi.org/10.1016/j.expthermflusci.2014.10.026

Ishak, M. H., Ismail, F., Mat, S. C., Abdullah, M. Z., Abdul Aziz, M. S., & Idroas, M. Y. (2018). Numerical analysis of nozzle flow and spray characteristics from different

nozzles using diesel and biofuel blends. *Energies, 12(2)*(281). doi:https://doi.org/10.3390/en12020281

Ishida, T., Maekawa, k., & Kishi, T. (2007). Enhanced modeling of moisture equilibrium and transport in cementitious materials under arbitrary temperature and relative humidity history. *Cement and Concrete Research, 37(4)*, 565-578. doi:https://doi.org/10.1016/j.cemconres.2006.11.015

Jamali, S. H. (2014). *Computational Modeling of Turbulent Ethanol Spray flames in a Hot Diluted Coflow*. Delft University of Technology.

Jungho, K. (2006). Spray Cooling heat transfer: The state of the art. *International Journal of Heat and Fluid Flow*, 753-767. doi:https://doi.org/10.1016/j.ijheatfluidflow.2006.09.003

Kim, T., & Park, S. (2018). Modeling flash boiling breakup phenomena of fuel spray from multi-hole type direct-injection spark-ignition injector for various fuel components. *Energy Conversion and Management, 160*, 165-175. doi:https://doi.org/10.1016/j.enconman.2018.01.042

Kristof, O., Bulejko, P., & Sverak, T. (2019). Experimental Study on Spray Breakup in Turbulent. *Processes, 7(12)*(911). doi:https://doi.org/10.3390/PR7120911

Kumar, N., & Puranik, B. P. (2017). Numerical study of convective heat transfer with nanofluids in turbulent flow using a Lagrangian-Eulerian approach. *Applied Thermal Engineering*, 1674-1681. doi:https://doi.org/10.1016/j.applthermaleng.2016.08.038

Lawing, P. L., & Kilgore, R. A. (1986). Cryogenic Wind Tunnels for High Reynolds Number Testing. *NASA Technical Memorandum*.

Lefebvre, A. H., & McDonell, V. G. (2017). *Atomization and Spray (Second ed.).* CRC Press. doi:https://doi.org/10.1201/9781315120911

Liu, H., Yan, P., Cai, C., Gao, J., & Yin, H. (2017). Numerical simulation on multiphase spray cooling. *IOP Conference Series. 100(1).* Earth and Environmental Science. doi:https://doi.org/10.1088/1755-1315/100/1/012082

Majaron, B., Aguilar, G., BasingeBrooke, Randeberg, L. L., Svaasand, L. O., Lavernia, E. J., & Nelson, J. S. (2002). Intermittent cryogen spray cooling for optimal heat. *Physics in Medicine and Biology, 47(18)*, 3275-3288. doi:https://doi.org/10.1088/0031-9155/47/18/301

Majaron, B., Aguilar, G., Basinger, B., Randeberg, L. L., Svaasand, L. O., Lavernia, E. J., & Nelson, J. S. (2001). Sequential cryogen spraying for heat flux control at the skin surface. *The International Society for Optical Engineering, 4244*, 74-81. doi:https://doi.org/10.1117/12.427777

Maruyama, S., & Moriya, S. (2021). Newton's Law of Cooling: Follow up and exploration. *International Journal of Heat and Mass Transfer, 164*(120544). doi:https://doi.org/10.1016/j.ijheatmasstransfer.2020.120544

Menter, F. R. (1993). Zonal Two Equation k-ω Turbulence Models for Aerodynamic Flows. *AIAA*.

Menter, F. R. (1994). Two-equation eddy-viscosity turbulence models for engineering applications. *AIAA Journal, 32(8)*, 1598-1605. doi:https://doi.org/10.2514/3.12149

Mudawar, I., & Estes, K. A. (1996). Optimizing and Predicting CHF in Spray Cooling of a Square Surface. *Journal of Heat Transfer*, 672-679. doi:https://doi.org/10.1115/1.2822685

Mugele, R. A., & Evans, H. D. (1951). Droplet Size Distribution in Sprays. *Industrial & Engineering Chemistry*, 1317-1324. doi:https://doi.org/10.1021/ie50498a023

Nelson, J. S., Milner, T. E., AnvarI, B., Tanenbaum, B. S., Kimel, S., Svaasand, L. O., & Jacques, S. L. (1995). Dynamic epidermal cooling during pulsed laser treatment of port wine stain. A new methodology with preliminary clinical evaluation. *Archives of Dermatology*, 695-700. doi:10.1001/archderm.131.6.695

Paciaroni, M., & Linne, M. (2013). Current Technological Advances in Fuel Spray Imaging. *IEEE Green Technologies Conference* (pp. 356-361). GreenTech. doi:https://doi.org/10.1109/GreenTech.2013.61

Rees, A., Araneo, L., Salzmann, H., Lamanna, G., Sender, J., & Oshwald, M. (2020). Droplet velocity and diameter distributions in flash boiling liquid nitrogen jets by means of phase Doppler diagnostics. *Experiments in Fluids, 61(18).* doi:https://doi.org/10.1007/s00348-020-03020-7

Reitz, R. D. (2007). A Photographic Study of Flash-Boiling Atomization. *Aerosol Science and Technology*, 561-569. doi:https://doi.org/10.1080/02786829008959370

Schmodt, D. P., Nouar, I., Senecal, P. K., Rutland, C. J., Martin, J. K., Reitz, R. D., & Hoffman, J. A. (1999). Pressure-Swirl Atomization in the Near Field. *Society of Automotive Engineers, Inc.* doi:10.4271/1999-01-0496

Senecal, P. K., Schmidt, D. P., Nouar, I., Rutland, C. J., Reitz, R. D., & Corradini, M. L. (1999). Modeling High Speed Viscous Liquid Sheet Atomization. *International Journal of Multiphase Flow, 25(6)*, 1073-1097. doi:https://doi.org/10.1016/S0301-9322(99)00057-9

Spraying Sytems Co. (2021). *Spray pattern & Nozzle type*. Retrieved from Spraying Systems Co.: https://www.spray-nozzles.co.za/applications/dust-control/spray-pattern-nozzle-type/

Tarantino, L., Goiorgi, M. G., Ficarella, A., & Laforgia, D. (2010). Numerical modelling of high-pressure cryogenic sprays. *AIAA Fluid Dynamics Conference*. doi:https://doi.org/10.2514/6.2010-5007

Toda, S. (1972). A study of mist cooling (1st report : Investigation of mist cooling). *Heat Transfer*, 39-50. doi:https://doi.org/10.1299/kikai1938.38.581

Toh, K. C., Yan, Z. B., Duan, F., Wong, T. N., Choo, K. F., Chan, P. K., & Chua, Y. S. (2010). Experimental Thermal and Fluid Science. *Applied Thermal Engineering*, 1225-1230.

Weber, C., & Dresden, T. (1931). Breakup of a liquid jet. *Texas Scholar Works*. doi:http://dx.doi.org/10.26153/tsw/3371

Wilcox, D. C. (2008). Formulation of the k-! Turbulence Model Revisited. *AIAA, 46(11)*, 2823-2838. doi:https://doi.org/10.2514/1.36541

Xue, R., Ruan, Y., Liu, X., Chen, L., Liu, L., & Hou, Y. (2019). Numerical Study of the Effects of Injection Fluctuations on Liquid Nitrogen Spray Cooling. *Thermodynamics: Modeling and Simulation, 7(9)*(564). doi:https://doi.org/10.3390/pr7090564

Xue, R., Ruan, Y., Liu, X., Chen, L., Zhang, X., Hou, Y., & Chen, S. (2018). Experimental study of liquid nitrogen spray characteristics in atmospheric environment. *Applied Thermal Engineering, 142*, 717-722. doi:https://doi.org/10.1016/j.applthermaleng.2018.07.056

Zapolski, D. P., Bilicki, Z., Bolle, L., & Franco, J. (1996). The non-equilibrium relaxation model for one-dimensional flashing liquid flow. *International Journal of Multiphase Flow, 22(3)*, 473-483. doi:https://doi.org/10.1016/0301-9322(95)00078-X

Zeng, Y., & Lee, C.-f. F. (2001). An Atomization Model For Flash Boiling Sprays. *Combustion Science and technology, 169(1)*, 45-67. doi:https://doi.org/10.1080/00102200108907839

Zhou, Z., Wu, W.-T., Chen, B., Wang, G.-X., & Guo, L. (2012). An experimental study on the spray and thermal characteristics of R134a two-phase flashing spray. *International Journal of Heat and Mass Transfer, 55(15-16)*, 4460-4468. doi:https://doi.org/10.1016/j.ijheatmasstransfer.2012.04.021

Zuber, N. (1959). *Hydrodynamic Aspects Of Boiling Heat Transfer (Thesis).* California: Physics and Mathematics. doi:https://doi.org/10.2172/4175511